

## **Inter-relationship between nuclei and gross characteristics of manganese nodules, Central Indian Ocean Basin**

Chiranjeeb Sarkar<sup>1</sup>, Sridhar D. Iyer<sup>2</sup> and Sugata Hazra<sup>3</sup>

1 Department of Geological Sciences, Jadavpur University, Kolkata 700 032, India

2 National Institute of Oceanography, Dona Paula, Goa 403 004, India

3 School of Oceanographic Studies, Jadavpur University, Kolkata 700 032, India

### **ABSTRACT**

More than 200 samples of manganese nodules from the Central Indian Ocean Basin (CIOB) were studied for their different parameters. The study included various aspects such as morphology, texture, mineralogy and composition of the nodules. The nuclei of the nodules were also examined along with the oxide layers. We attempt to correlate the nucleus (their type and abundance) with the nodule parameters such as their external morphology, chemical composition, and suitable location of formation, amongst others. We found various nucleating materials and these include rock fragments (fresh and altered), clay, pumice and sharks' teeth. In a majority of the cases rock fragments are dominant in the core of the nodules and these conform to that of the seafloor basalts. The shape of the nuclei influences that of the nodules especially during their initial period of growth. Irrespective of the kind of nuclei, todorokite is the main mineral of the nodules. The nodules of the CIOB were formed mostly due to hydrogenous accretion of ferromanganese oxides while diagenetic contribution of metals is less common.

**Keywords:** Manganese nodules, Central Indian Ocean Basin, nucleus, todorokite, hydrogenous accretion, diagenetic

## INTRODUCTION

Resource estimates have shown that the manganese nodule-bearing basin in the Indian Ocean represent the second largest nodule rich area after the Equatorial North Pacific Belt (Siddiquie et al., 1978, Cronan,1980). This basin, identified as the Central Indian Ocean Basin (CIOB), is roughly bounded between lat. 10° and 16° 30' S and long. 72° and 80° E and is on an average 5000 m deep. The nodules are found mainly in two forms: (i) as concretions in deeper waters (>5000 m) at the sediment-water interface, and (ii) as crusts on the summits and slopes of submarine elevations abyssal hills and seamounts. Martin-Barajas et al. (1991) reported that favourable conditions for the hydrogenetic growth of nodules in the CIOB began in Late Miocene/Early Pliocene while diagenetic nodules formed since Late Pliocene.

It is well recognised that several unambiguous factors favour the initiation, growth and distribution of nodules at abyssal depth (e.g., Glasby et al., 1983, 2000; Mukhopadhyay et al., 2002). These parameters are: an abyssal hill topography, water depth >4500 m, a low sedimentation rate in the order of a few mm/1000 yr, an effective bottom water current to remove the sediment veneer from the nodule surface, availability of sufficient seed or nuclei material, an overall oxidising condition, biological productivity and supply of metals that are precipitated from the seawater and also through a process of remobilisation from the underlying sediment.

Information exists on the CIOB pertaining to the relationship between morphology and composition (Jauhari, 1990) and between size and geochemistry of nodules (Valsangkar and Ambre, 1994), amongst others. But in these studies the nucleus of the nodules were either removed during the analyses or else not considered in-depth as the nucleus was not the subject of those authors' investigations. Martin-Barajas et al. (1988) identified three main types of nuclei in the CIOB nodules. These were altered ash layer fragments, red clay indurated sediments and rhyolitic pumice. Besides these, the authors also identified altered basalt fragments, fragmented nodules or crust, sharks' teeth and turbiditic indurated sediments that form minor and isolated types of nuclei. So far, there has been no attempt to correlate the different nuclei with the gross parameters of the nodules. Hence, our present endeavour is to investigate the nucleus (their type and

abundance) and determine if any linkage exists between these and the nodule parameters such as their external morphology, chemical composition, grade, abundance and location of formation.

## **METHODOLOGY AND SAMPLE PREPARATION**

We examined 208 nodules and 7 encrustations recovered from the CIOB (Table 1) for their form, size, surface texture, abundance and the nucleus type (Table 2). We selected 171 samples for further detailed study and their dimensions (length, breadth, thickness) were measured and the surface textures were noted. The type of nucleus in sliced samples was determined. The thickness of the oxide layer and the nucleus were measured. Since the oxide layer was non-uniform, the thickness was measured at three areas and then averaged (Table 3). Photographs of nodules of different shape, size ranges and surface textures were obtained. Thirty samples were selected for reflected light Microscopy, X-Ray Diffraction (XRD), Scanning Electron Microscope (SEM) and Energy Dispersive Spectrometer (EDS) studies.

## **RESULTS AND INTERPRETATION**

### **Morphology**

Generally, the nodules display a variety of forms that can be distinguished by studying their morphological features. Meyer (1973) classified the nodules from the North Pacific by detailing several morphological parameters such as external shape, size, surface texture, symmetry of laminations and a relative tendency to occur intergrown (i.e., in a multinucleate, poly-lobate configuration). But usually the nodules are classified on the basis of size, shape and surface texture.

In the CIOB the size of nodules varies from <10 mm to several cm. The selected samples show a size range from <2 to >8 cm while a few are >10 cm (Fig. 1). Among all the samples 1.18% were very small (<2 cm), 22.80% were small (2-4 cm), 52.63% were medium (4-6 cm), 15.79% were large (6-8 cm) and the remaining 7.6% were very large (>8 cm) (Fig. 2). Therefore, the dominating size range is between 4 and 6 cm (Table 2). Depending on depth and environment of formation,

larger and smaller nodules may occur in a mixed population. The nodules recovered from different locations in the CIOB were inspected and characteristically the specimens from individual sites show a remarkable similarity in their size and external morphology. At some sites the nodules are small and numerous but larger ones are less, while at other sites mostly larger nodules occur while smaller ones are sporadic.

The nodules commonly are spheroidal to sub-spheroidal and elongated in shape. Apart from these discoidal, tabular, polygonal, potato shaped, small botryoidal type, cannon ball-like and irregular nodules are not uncommon (Fig. 3). Many of these shapes are similar to nodules recovered in other oceans (Glasby et al., 1983; Friedrich et al., 1983). Generally, the small sized nodules are spheroidal and as the size increases the sphericity decreases. An increase in size appears to lead to an increase in irregularity, and therefore, the sphericity of a nodule is inversely proportional to its size. The larger nodules generally tend to be poly-nucleated and this may result from two stage of deposition of ferromanganese (Fe-Mn) oxides. Also, plausibly due to bottom water currents the smaller nodules on the seafloor may roll and get attached. Such joined nodules could accrete Fe-Mn oxides at a later stage and form a larger poly-nucleated nodule.

The external surface of the CIOB nodules is commonly ornamented by mammillae of different size and relief. Overall, the nodules display a smooth or rough to gritty surface but several nodules have an intermediate texture (Fig. 4). Of the nodules that we studied, about 52% have a rough surface, 26% show a smooth surface while the others exhibit both kinds of surface (Fig. 5; Table 2). In general, the larger the nodule, the greater is the likelihood of surface variations between the top and bottom. It is presumed that the relatively clean and smooth surface of the nodules represent the top whilst the comparatively rough surface with pronounced biological activity corresponds to the bottom (Goodell et al., 1971; Raab, 1972; Halbach et al., 1975). This is because the sediment and biodebris deposited on the nodules tend to be washed off while the bottom portion being embedded within the sediment may be burrowed and bored by bottom-dwelling organisms. Furthermore, the upper portion of the nodule obtains hydrogenetic precipitation of metals from the

sea water while the lower is formed by diagenetic remobilisation of metals through the host sub-oxic sediments.

The nodules with rough surface have mammillae of higher relief and size, are sediment infilled and show prolific biological activity indicative of the surface being in contact with the host sediment. Also, such nodules are difficult to break than those with smooth surface. Worm tubes and channels mostly occur in the depressed part of the rough side. The equatorial rim or knobby band, clearly exhibited by some nodules, contains numerous mammillae of high relief.

### **Nucleus Type**

A nucleus is essential for the initiation, growth and spread of nodules. The size, shape and composition of the nucleus may to a large extent influence the morphology and the bulk chemical composition of the nodules. In a majority of cases rock fragments, derived from seamounts, abyssal hills and fracture zones act as nucleus (Glasby, 1973, Horn et al., 1973; Iyer and Sharma, 1990; Mukhopadhyay et al., 2002). The other most common nucleating materials are palagonite, clay, shark teeth and even parts of older nodules and crust. Among the selected CIOB nodules, we observed that altered basalt comprises 56.15%, clay (mainly palagonite) 17.54%, fresh basalt 12.3%, sharks' teeth 3.51%, pumice 2.34%, poly-nucleated 5.26 % and the remaining 2.92 % are unidentified (Figs. 6, 7; Tables 2, 3). The external form of the nucleus determines the nodule shape, for instance triangular shaped nodules have sharks' teeth (Fig. 7b) as nuclei. In the case of the CIOB nodules, most of the rock fragments acting as nuclei could be directly related to the seamounts that are common in the basin (Das et al., 2005). Therefore, it appears that the seamounts also influence the abundance of nodules by way of contributing nucleating materials. We noted that areas that host nodules of uniform size, shape and distribution generally have a similar kind of nuclei.

### **Internal Features**

An examination of sectioned nodules revealed three prominent zones: the nucleus, an altered zone and Fe-Mn oxide layers of variable thickness. The layers

vary within a single nodule as well as in different nodules with different nucleus and thus, indicate a change in the accretion rates of the Fe-Mn oxides. The average thickness of the layers and of the nucleus were measured (Table 3) and the oxide : nucleus ratio was plotted for the nodules with different nuclei. The plots show a negative trend for each nucleus type except for a crude positive correlation for the sharks' teeth and this may probably be due to the symmetrical nature of the sharks' teeth.

The oxide : nucleus ratio also varies for the nodules collected from different topographic areas. The nodules near the summit of seamounts have the lowest oxide : nucleus ratio, it increases for the nodules along the seamount flank and is highest for nodules from the abyssal plain (cf. Mukhopadhyay, 1988). The oxide : nucleus ratio also increases as the size increases, possibly due to an extra source of supply of oxides from the host sediments. The nature of nuclei also seems to be topography-dependent. Close to the seamount summit the nodules are mono-nucleate and composed largely of indurated sediment and rock fragments whereas nodules from foothills and deeper regions are both mono- and poly-nucleate and their nuclei are of altered rocks, indurated clays and older nodules. Interestingly, this difference is also reflected in the surface texture and composition of the nodules. The smooth textured nodules from the summit show high Fe and Co whereas rough textured nodules from the plain are enriched in Mn, Ni and Cu.

Most nodules display prominent conformable layers which represent the concentric shell structure. The thickness of the layering may vary from several micrometers to several millimeters. The gross layering, so called to distinguish it from the delicate thin laminations, is visible due to its reflectivity difference with the adjacent layer or because of the presence of thin clay-rich partings between the layers. The inner layers tend to conform to the shape of the nucleus but away from the core, the layers follow the shape of the core less and less closely. A microscopic study of these laminations revealed several textural zones.

As was also noted by Cronan and Tooms (1968) for Carlsberg Ridge nodules, the botryoidal surface of nodules appears as colloform layers under the microscope and the layers vary in denseness and continuity (Fig. 8a, b). The contact between

different layers may be sharp in places and diffuse in others. The elliptical columnar texture shows a colloform nature and consists of sub-concentric laminae which progressively widen outwards (Fig. 8c). The presence of alternate laminae in a columnar texture could be attributed to two different sources of Fe-Mn oxides, i.e., seawater in case of Fe-rich layers and interstitial water in case of Mn-rich layers. Furthermore, the nodules show diagenetic features such as fractures filled with Fe-Mn oxides from the host sediment.

Based on Foster's Zone Classification (1972), the commonly seen major internal features of the nodules were categorised.

- (i) The 'massive zone' is a dense unit of predominantly regular but diffuse laminae of intergrown microcrystalline todorokite and birnessite, with a minor amount of clastic debris (Fig. 8b).
- (ii) The 'mottled zone' is characterised by a chaotic layering of crystalline todorokite and birnessite and amorphous Fe oxides. The massive and mottled zones contain the greatest proportion of crystalline material and the greatest amount of Mn, Ni and Cu. (see also Raab, 1972).
- (iii) The 'compact zone', texturally similar to the massive zone, is mainly composed of well defined highly reflective X-ray crystalline laminae.
- (iv) The 'columnar zone' consists of radially oriented columns of X-ray amorphous material (Fig. 8c). Clay occurs between the adjacent columns. The laminae composing the columns display a colloform texture and each column typically shows a dendritic pattern. In places the radial columns are short, densely packed and relatively uniform laterally, giving a concentrically layered appearance. These laminated and columnar zones have higher Fe content. In these layers there are abundant remnants of radiolaria as well as angular rock fragments. In several nodules one or all of the above zones occur.

The general internal structural patterns are unique in the nodules collected from different sites. As examples, the nodules from the abyssal plain show a prominent well-developed columnar-cusate like structure whereas those from abyssal hill show parallel laminations.

Under the SEM the concentric growth or a cusped structure with alternate laminae of Mn and Fe-rich layer was very evident. At times a single cusp shows variation in thickness being greater at the crest and gradually decreases towards the limb (Fig. 9a). The variation in micro-laminae is responsible for different mineral phases of Fe-Mn oxides. The interior of the nodules shows aggregates of small and large botryoids composed of flocculated material (Fig. 9b). These botryoids show cusped and columnar forms in cross section and have small balls of clay as nuclei (Fig. 9c) and are made up of amorphous Mn and Fe hydroxides.

The CIOB nodules show dendritic, columnar laminations with Mn- rich light and Fe-rich dark bands. The inner layers (closer to the nucleus) are rich in Fe and Co whereas the outer layers have a high concentration of Mn, Ni and Cu (Table 4). This fact could indicate formation of the nodules by two different processes i.e., the inner layers may have formed largely by hydrogenous process while the outer layers formed by diagenetic re-mobilisation of metals (Banerjee et al., 1991).

The presence of well-developed todorokite crystals in a crevice of a nodule is indicative of intra-nodule diagenesis (Fig. 9d). Biological remnants in the form of benthic foraminiferal tubes were also identified. The nuclei also contain phillipsite crystals (Fig. 10a) some of which show dissolution. Crystals of todorokite and zeolites sometimes occur together. When todorokite is present in well crystalline forms then birnessite or  $\delta$ -MnO<sub>2</sub> appeared as hay-stacks (Fig. 10b). Pumices that occur as nuclei in nodules show typical glass flow structure (Fig. 10c). The clayey nucleus made up of montmorillonite at times shows dehydration cracks.

## **Mineralogy**

The mineralogy is not uniform throughout the oxide layers of a single nodule and consists of three kinds of minerals: 10 Å manganite (todorokite), 7 Å manganite (birnessite) and  $\delta$ -MnO<sub>2</sub>. The Fe phases are amorphous but in a few specimens the presence of goethite and ferrihydrate are suspected. In addition there are some accessory minerals such as quartz, clay, feldspar and phillipsite. The Mn minerals



are not easily distinguishable under the ore microscope but todorokite has a relatively higher reflectivity than  $\delta$ -MnO<sub>2</sub>. XRD of selected samples confirm the presence of todorokite that indicates the replacement of the nucleus. It has been reported that the intensity and crystallinity of todorokite increase with water depth in the CIOB (Rao, 1987). SEM studies revealed elongated and stumpy crystals of todorokite (Fig. 9d) and blade-like crystals of birnessite (Fig. 10b) in some samples. Generally, the CIOB nodules have a low crystallinity and abundant amorphous minerals.

The morphological features of the nodules seem to have a certain control over the mineralogy. The rough surface nodules, abundant in the siliceous sediment, have todorokite as the main mineral phase whereas the smooth surface nodules, common in the pelagic clay, have  $\delta$ -MnO<sub>2</sub> (cf. Rao, 1987). But for some differences in abundance of the minerals, the XRD patterns were found to be quite similar irrespective of the nucleus type.

XRD of the nucleus show the dominant minerals to be plagioclase, quartz and phillipsite. XRD of some samples show the dominance of quartz in pumice that occurs as a nucleus, while plagioclase (labradorite-andesine) is the dominant mineral in nodules that have a basaltic core. The specimen of ferromanganese crust is largely composed of amorphous Fe-Mn minerals and there hardly exists any identifiable peak in the XRD profiles.

Todorokite is the major mineral phase in the CIOB nodules that are normally associated with siliceous sediment with high to moderate biological productivity (Jauhari and Pattan, 2000). It is suggested that the supply of bivalent ions Ni, Cu, Zn etc. from the host sediment during diagenesis leads to formation and stabilisation of todorokite. An increase in biological productivity would facilitate an enhanced supply of these ions to the sediment and thus, influence the growth of todorokite (Glasby and Thijssen, 1982).

At relatively shallow water depth highly oxidised  $\delta$ -MnO<sub>2</sub>, birnessite and FeOOH remain the predominant manganese and iron bearing phases in the nodules.

These nodules, found in southern part of the CIOB in the pelagic clay area where the biological activity is low, contain phillipsite, illite and sometimes remnants of benthic foraminifera. These facilitate incorporation of Co and Pb in greater amount into  $Mn^{+4}$  in birnessite and  $Fe^{+3}$  in  $FeOOH$  (Burns and Burns, 1977). Thus, biological productivity, mineralogy and chemical composition seem to be interlinked.

### **Chemical Composition**

Nodules have a variable chemical composition that may be due to, among other things, location of nodule occurrence, topography and the depositional environment.

The grade of the CIOB nodules, determined by  $Cu + Ni + Co$  content (wt%), on an average is better than 2%. It has been observed that the grade is inversely proportional with abundance (Sudhakar, 1988). Another interesting feature is the inverse relationship between Fe and Mn that may be due to the difference in the source of Mn and Fe. Nodules from hill tops have highest Fe in contrast to those from the plain that have the lowest while Mn shows a contrasting behaviour. Ni and Cu correlate positively with Mn but Co sometimes shows some positive correlation with Fe (Kodagali and Sudhakar 1993). The Mn/Fe ratio in the adjacent growth layer to the nucleus is around 1.5 indicating a hydrogenetic source; while the outer layers, with Mn/Fe ratio between 4.2 and 5.4, are indicative of early diagenesis (cf. Halbach et al., 1981). This variation in source suggests that rates of accretion and environmental condition during formation of the layers were different.

The chemical composition of nodules also depends on nodule size, bottom sediment type, surface texture and nearness to structural and/or topographic features (fracture zones, seamounts). Nodules from siliceous sediment are smaller in size, show a rough texture, have todorokite, are rich in Mn, Cu, Ni and Zn and have  $Mn/Fe > 4$ . These characteristics suggest an early diagenetic origin. In contrast, nodules from red clay areas are rich in Fe, Co, Ti and P and have  $Mn/Fe$  ratio  $< 2.5$  that points to a hydrogenous metal source (Mukhopadhyay et al., 2002). Rare earth elements are highly enriched in these nodules and are generally carried by a single

authigenic phase (viz., titanium-rich ferriphosphate) consisting of Fe-Ti-P and again indicate a hydrogenous source (Pattan and Banakar, 1993).

The topography also influences the chemical variation of the nodules. Nodules sporadically distributed on seamount summits and upper slopes are characterised by low Mn/Fe (<3), low Ni+ Cu (1.88%), low Fe (9.36 %) and Co (0.116 %) and with oxide : nucleus ratio <1. The nodules on plain area have high Mn/Fe (>4), high Ni+ Cu (>2.5%), lowest Fe and Co with oxide : nucleus near to 1. In valley areas the nodules are characterised by lowest Mn/Fe (<2), lowest Ni+ Cu (<1.5%), higher Fe (10.5 %) and Co (0.14 %) (Mukhopadhyay and Nath, 1988).

The average chemical composition correlates well with nodule size in that nodules of specific size group (< 2 to 4 cm) display a similar composition. For instance, small to medium size nodules (<2 to 4 cm) have high Mn, Cu, Ni, Mn/Fe and Cu+ Ni+ Co while the larger nodules have high Fe but Co and Zn remain almost constant (Valsangkar et al., 1992).

In the biologically productive area, siliceous and calcareous plankton tend to incorporate trace metals in their skeletal parts and these trace metals are released to the seafloor (in the case of calcareous plankton below the carbonate compensation depth) by the settling organisms and thus enrich the interstitial waters of the sediments with trace metals (Aplin and Cronan, 1985). During post-depositional process the metals are diagenetically included in the growing nodules. In areas of high productivity the redox potential decreases and subsequently precipitation of  $Mn^{+2}$  is facilitated and todorokite crystallizes. The uptake by todorokite of Ni, Cu and Zn stabilises its crystal structure. In contrast,  $\delta$ - $MnO_2$  rich nodules are rich in Fe and Co (Jauhari and Pattan, 2000).

EDS analyses were carried out to determine the gross chemistry of the nucleus and of the oxide layers. Table 4 shows an analysis of a nodule that has altered basalt as a nucleus as evident from the high content of  $SiO_2$  (53%) and high  $Fe_2O_3$ . Furthermore, MnO, NiO and CuO gradually increase towards the boundary. The sample also shows chemical variation on both sides of a cusp. For instance, the

inner cusp has high SiO<sub>2</sub> and lower MnO vis-à-vis the outer cusp that has lower SiO<sub>2</sub> and higher MnO.

A ferromanganese crust with botryoids was analysed. The EDS result reveals the characteristic presence of high Fe<sub>2</sub>O<sub>3</sub> and low MnO (Table 5). In an exposed section of a botryoid the presence of CoO is very conspicuous. The EDS result **on** a pumice occurring as a nucleus shows a predominance of SiO<sub>2</sub> followed by Al<sub>2</sub>O<sub>3</sub> and with very little of Fe<sub>2</sub>O<sub>3</sub> and MnO (Table 6). The analysis of an unaltered basaltic nucleus shows high ferromagnesian and low silica contents (Table 7).

The bulk composition of the nuclei of nodules reflects the common trend of weathering of oceanic basalts where concentration of Si, Al and Ti remain less affected. The close similarity in the average SiO<sub>2</sub> (55.2%), Al<sub>2</sub>O<sub>3</sub> (17%), Na<sub>2</sub>O (3.3%), TiO<sub>2</sub> (1.6%) and P<sub>2</sub>O<sub>5</sub> (0.1%) concentrations of the bulk nucleus and the CIOB seamount rocks suggest the derivation of nuclei from the several seamounts that occur in the CIOB (Iyer and Sharma, 1990; Das et al., 2005). There is some geochemical affinity of the nodule nuclei with the Indian Ocean Mid-Ocean Ridge Basalts but their origin from those ridges is unlikely because of the anhedral and subhedral morphology of the plagioclase grains forming the nuclei (Banerjee and Miura, 1998).

Geochemical studies of nodules and encrustations from various basins of the Indian Ocean and from different topographic domains display a wide variation that could be directly attributed to the difference in source of metals to the accreting nodules. The CIOB nodules generally have accreted hydrogenetically and show a tendency towards early diagenetic growth which includes an intermediate type (Mukhopadhyay et al., 2002). The nodules from the abyssal plain have high Mn/Fe ratio, Cu and Ni, while those from elevated areas have high Fe and Co and low Mn/Fe ratio. These studies show that abyssal hill topography could influence sedimentation rates and oxidation state which in turn affect the distribution, morphology and chemistry of the nodules.

## DISCUSSION

In this study, we have examined several aspects of the CIOB nodules and their inter-dependence are now discussed.

The nuclei are heterogeneous but are mainly of rock fragments that are compositionally similar to the seafloor basalts. Hence, the source of these nuclei (both fresh and weathered) could be the volcanics derived from intra-plate eruptions that produced the seamounts and abyssal hills. The diverse external morphology of the nodules is directly related with that of the nucleus morphology. In terms of the overall shape, it is observed that the smaller nodules show more similarity with their nucleus and as the nodules grow larger this resemblance gradually decreases and the nodules tend to attain a sub-spheroidal to elongated shape. The oxide : nucleus ratio has a poor relationship with the type of nucleus but has a good correlation with the topography. The abyssal plain nodules have a greater thickness (a few cm) of oxide layer irrespective of nucleus type than the nodules (a few mm) of seamount summits and flanks. This is because in the former case there is an additional source of metals through diagenesis.

Conformable laminations and similarity in thickness of the gross layering (Fig. 8a, b) around a nucleus suggest repetitive deposition of metals irrespective of source. Mn-rich laminae are attributed to a source from interstitial pore water during diagenetic remobilisation. The other diagenetic features commonly present are cracks, fractures filled with secondary Fe-Mn oxides, etc. During the process of diagenesis the composition of the different layers tends to change and in due course of time may get homogenised. This phenomenon of 'resetting of the clock' in nodules creates a problem in determining the exact age of a nodule that formed due to a constant deposition rate of metals (Roy, 1981). The internal structures of nodules are also controlled by the topography. For instance, the nodules from abyssal plains show a prominent well-developed columnar to cusped form whereas the abyssal hill nodules show parallel laminations.

Irrespective of the type of nucleus, the dominant mineralogy of the nodules studied is well crystallised todorokite while birnessite is less common and  $\delta$ -MnO<sub>2</sub> is rare and poorly crystalline. The mineralogy is not uniform throughout the oxide layers since todorokite dominates over  $\delta$ -MnO<sub>2</sub> in the marginal layers. Therefore, the process of accretion of oxides is more influential in controlling the mineralogy rather than the type of nucleus.

The geography, topography, the process of formation, bottom sediment type, vicinity of seamounts etc. play a combined role in determining the chemical composition of the nodules. The Mn/Fe ratio gradually increases from near the nucleus to the outer layer suggesting a change in source of the metals as the nodules grow larger. The type of surface texture is diagnostic of the source of metals i.e., hydrogenous or diagenetic. Normally the CIOB nodules show a mixed type of origin. Their top smooth part is mainly formed by the hydrogenetic precipitation from seawater and the bottom rough part is formed by diagenetic remobilisation of metals through the sediment column.

## CONCLUSIONS

A study of over 200 nodules and a few crusts recovered from the CIOB has led to the following inferences.

1. Nodules of variable size, shape and surface texture occur in the study area. The most dominant size class is 4-6 cm and the shapes are spheroidal, sub-spheroidal and elongated and the texture ranges from smooth to rough.
2. The nucleus plays a most crucial role in the formation of the nodules. The shape of the nuclei seems to control the shape in the early stages of growth of the nodules. But once the growth is initiated then enrichment of metals is solely controlled by the depositional process and the environment of formation. In most cases altered basaltic fragments or clay form the nuclei.
3. The nucleus : oxide ratio varies with topography and is independent of the type of nucleus.

4. A smooth surface texture is produced due to hydrogenous precipitation of Fe-Mn oxides from the sea water while a rough surface is mainly due to diagenesis of metals from the host sediment.
5. Mineralogy (mainly todorokite) of the various types of nodules is similar irrespective of type of nucleus.
6. The chemical composition, abundance and grade of the nodules are primarily controlled by the depositional process and not necessarily by the type of nucleus.

## **ACKNOWLEDGEMENTS**

This paper forms a part of the Master's degree of the first author. We thank the Director (NIO), the Vice-Chancellor (JU) and Head of the Department of Geological Sciences (JU) for permission to carry out this joint study. We acknowledge Dr. M. Shyam Prasad and S. Jaishankar for providing details of the sample locations from the project's data bank. G. Prabhu, V. M. Khedekar and R.N. Uchil helped during the XRD, SEM-EDS and DTP work. An in-depth review by an anonymous referee and the encouragement of Prof. S.P. Varnavas are highly appreciated. This is NIO's contribution # 4310

## REFERENCE

- Aplin, A.C. and Cronan, D.S., 1985. Ferromanganese oxide deposits from the Central Pacific Ocean, II. Nodules and associated sediments. *Geochimica et Cosmochimica Acta* 49: 437-451.
- Banerjee, R. and Miura, H., 1998. Mineral chemistry, bulk composition and source of the ferromanganese nodules nuclei from the Central Indian Ocean Basin. *Geo-Marine Letters*, 18, 66-69.
- Banerjee, R., Iyer, S.D. and Dutta, P., 1991. Buried nodules and associated sediments from the Central Indian Basin. *Geo-Marine Letters*, 11, 103-107.
- Burns, R.G. and Burns, V.N., 1977. Mineralogy. In: *Marine Manganese Deposits*, Glasby G.P. (ed.), Elsevier, Amsterdam, 185-248.
- Cronan, D.S., 1980. *Underwater Minerals*. Academic Press, Oxford, 363 pp.
- Cronan, D.S and Tooms, J.S., 1968. A microscopic and electron probe investigation of manganese nodules from the northwest Indian Ocean. *Deep-Sea Research*, 15, 215-223.
- Das. P., Iyer. S.D., Kodagali. V.N., Krishna. K.S., 2005. Distribution and origin of seamounts in Central Indian Ocean Basin. *Marine Geodesy*, 28, 259-269.
- Friedrich, G., Glasby, G.P., Thijssen, T. and Pluger, W.L., 1983. Morphological and geochemical characteristics of manganese nodules collected from three areas on an equatorial Pacific transect by R.V. Sonne. *Marine Mining*, 4, 167-254.
- Foster, A.R., 1972. Growth history of manganese nodules from the Baja California Seamount Province (Abst). *Acta Mineralogica-Petrographica Szeged*, 20, 384-386.
- Glasby, G.P., 1973. Distribution of manganese nodules and lebensspuren in underwater photographs from the Carlsberg Ridge, Indian Ocean. *New Zealand Journal of Geology and Geophysics*, 16, 1-17.



Glasby, G. P., 2000. Manganese: predominant role of nucleus and crust. In Schulz, H. D., Zabel, M. (Eds.), *Marine Manganese Geochemistry*. Springer-Verlag, Heidelberg, pp. 335-372.

Glasby,, G.P., Thijssen, T., 1982. Control of the mineralogy and composition of marine manganese nodules by the supply of divalent transition metal ions. *Neus Jahrbuch. Furmin.*, 145, 291-307.

Glasby,, G.P., Stoffers, P., Sioulas, A., Thijssen, T., Friedrich, G., 1983. Manganese nodule formations in the Pacific Ocean: a general theory. *Geo-Marine Letters*, 22, 47-53.

Goodell, H.G., Meylan, M.A. and Grant, B., 1971. Ferromanganese deposits of the South Pacific Ocean, Drake Passage, and Scotia Sea. In: Reid, J.L. (ed.) *Antarctic Oceanology, I. Antarctic Research Series*, Amer. Geophy. Union, Baltimore, 27-92.

Halbach, P., Ozkara, M. and Hense, J., 1975. The influence of metal content on the physical and mineralogical properties of pelagic manganese nodules. *Mineralium Deposita*, 10, 397-411.

Halbach, P., Sherhag, C., Hebich, V. and Marchig, V., 1981. Geochemical and mineralogical control of different genetic types of deep-sea nodules from the Pacific Ocean. *Mineralium Deposita*, 16, 58-84.

Horn, D.R., Horn, B.M. and Delach, M.N., 1973. Factors which control the distribution of ferromanganese nodules. National Science Foundation, Washington, Technical Report, 8, NSF GX 33616, IDOE-NSF, pp. 20.

Iyer, S. D. and Sharma, R., 1990. Correlation between occurrence of manganese nodules and rocks in a part of the Central Indian Ocean Basin. *Marine Geology*, 92, 127-138.

Jauhari, P., 1990. Relationship between morphology and composition of manganese nodules from the Central Indian Ocean. *Marine Geology*, 92, 115-125.

Jauhari, P. and Pattan, J. N., 2000. Ferromanganese deposits in the Indian Ocean. In Cronan, D. S. (Eds.), *Handbook of Marine Mineral Deposits*. CRC Publications, New York, pp. 171-195.

Kodagali, V.N. and Sudhakar, M., 1993. Manganese nodule distribution in different topographic domains of the central Indian Basin. *Marine Georesources Geotechnology*, 11, 293-309.

Martin-Barajas, A., Lallier-Verges, E. and Leclaire, L., 1991. Characteristics of manganese nodules from Central Indian Basin: relationship with sedimentary environment. *Marine Geology*, 101, 249-265.

Martin-Barajas, A., Lallier-Verges, E. and Leclaire, L., 1988. Origin of manganese nodule fields related to the geodynamic evolution of the central Indian Basin. *C.R. Acad. Sci. Paris*, 307, 1259-1264.

Meyer, K., 1973. Surface sediment and manganese nodule facies encountered by R/V Valdivia cruises 1972/73. In: Morgenstein, M. (ed.), *The origin and distribution of manganese nodules in the Pacific and prospects for exploration*. Intern. Symp. Hawaii Inst. Geophys., 125-136.

Mukhopadhyay, R., 1988. Morphological and geochemical studies of Polymetallic nodules from four sectors in the Central Indian Ocean Basin between 11° S and 16° S latitude. Unpublished PhD thesis, University of Calcutta.

Mukhopadhyay, R. and Nath, B. N., 1988. Influence of seamount topography on the local facies variation in ferromanganese deposits in the Indian Ocean. *Deep-Sea Research*, 35, 1431-1436.

Mukhopadhyay, R., Iyer, S.D., Ghosh, A.K., 2002. The Indian Ocean nodule field: petrotectonic evolution and ferromanganese deposits. *Earth-Science Review*, 60, 67-130.

Pattan, J.N. and Banakar, V.K., 1993. Rare earth elements distribution and behaviour in buried nodules from the Central Indian Basin. *Marine Geology*, 112, 303-312.

Raab, W.J., 1972. Physical and chemical features of Pacific deep sea manganese nodules and their implications to the genesis of nodules. In Horn, D.R. (Eds.), *Ferromanganese Deposits on the ocean floor*. MSF, Washington D.C., pp. 31-49

Rao, V.P.C., 1987. Mineralogy of polymetallic nodules and associated sediments from the Central Indian Ocean Basin. *Marine Geology*, 74, 151-157.

Roy, S., 1981. *Manganese deposits*. Academic Press, London, UK, 458 pp.

Siddiquie, H.N., Dasgupta, D.R., Sengupta, N.R., Srivastava, P.C., Mallik, T.K., 1978. Manganese iron nodules from the Indian Ocean. *Indian Journal of Marine Sciences*, 7, 239-253.

Sudhakar, M., 1988. Relation between grade and abundance of manganese nodules. *Current Science*, 57, 662-663.

Valsangkar, A.B. and Ambre, N.V., 1994. Relationship between size and geochemistry of polymetallic nodules from the Central Indian Ocean Basin: Significance in selection of high grade nodules. *Ocean technology: Perspectives*. Sushil Kumar, Agadi, V.V., Das, V.K. and Desai, B.N. (eds.), Publ. and Info. Dir., New Delhi, India, 827-841.

Valsangkar, A.B., Karisiddaiah, S.M. and Parthiban, G., 1992. Variation in size, morphology and chemical composition of polymetallic nodules from the Central Indian Ocean Basin. *Oceanography of the Indian Ocean*. Desai, B.N. (ed.), Oxford & IBH, 561-571.

## Caption of figures

- Fig. 1: Classification of nodules based on their size  
a: < 2 cm; b: 2-4 cm; c: 4-6 cm; d: 6-8 cm; e: >8 cm
- Fig. 2: Nodule size analysis
- Fig. 3: Classification of nodules based on their shape  
a: Rounded; b: Sub-rounded; c: Discoidal; d: Angular;  
e: Mammillated; f: Poly-nucleated
- Fig. 4: Classification of nodules based on surface texture  
a: Gritty; b: Intermediate; c: Smooth
- Fig. 5: Abundance of nodules with different surface textures
- Fig. 6: Nodule nucleus analysis
- Fig. 7: Classification of nodules based on type of nucleus  
a: Altered basalt; b: Sharks' teeth; c: Palagonite
- Fig. 8: Internal growth layers of nodules  
a: Electron microscopy shows cusps of variable thickness of FeMn oxides.  
b: Photomicrograph of a polished nodule depicting dense layers of todorokite and birnessite that form the massive zone. Some well developed colloform structures are evident on the top which are identified as laminated zone. Mag x400.  
c: Photomicrograph of a polished nodule displaying intricate curved laminae of Mn and Fe rich layers representing sections through botryoids. White or light grey laminae are Mn rich and dark grey laminae are amorphous Fe. Mag x400.

- Fig. 9: Electron micrographs of nodules
- a: The thickness of the cusp is maximum at the crest and gradually decreases towards limb.
  - b: Typical botryoidal feature within a nodule.
  - c: Cusps surrounding an earlier formed botryoid that has clay as nucleus.
  - d: A crystal of todorokite.

- Fig. 10: Electron micrographs of nodules
- a: An agglomeration of phillipsite crystals. Note the features of dissolution on some of the crystals.
  - b: Typical blade-like birnessite crystals.
  - c: Silicic glass flow structure in a pumice.

## Caption of tables

- Table 1: Details of sites from where samples were collected for this study.
- Table 2: Description of the studied nodules.
- Table 3: Detailed morphology of the selected nodules L-length, W-width, T-thickness, AB-altered basalt, B-basalt, C-clay, U- unidentified, ST-sharks' teeth, P-pumice.
- Table 4: a: EDS analyses of a nodule from nucleus to boundary. The numbers at the top indicate the layers away from the nucleus.  
b: EDS analysis of a cusp on either side of a nucleus.
- Table 5: EDS analysis on various areas of botryoids on a ferromanganese crust.
- Table 6: EDS analysis of a pumice as a core in a nodule.
- Table 7: EDS analysis of a fragment of basalt in the core of a nodule. The numbers indicate different parts of the sample. 1 : on a rough part, 2 : at a corner, 3 : on a smooth surface.

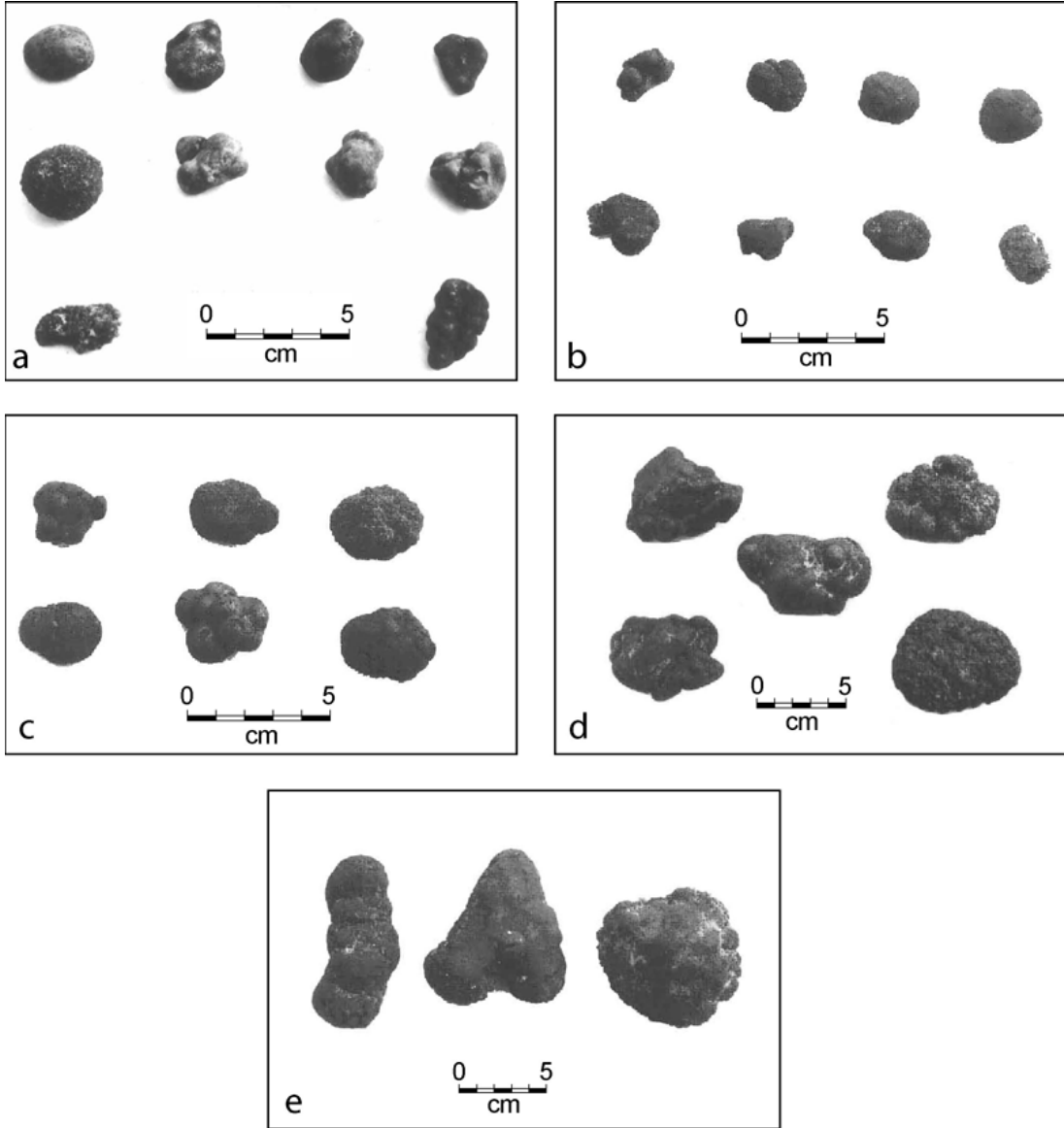
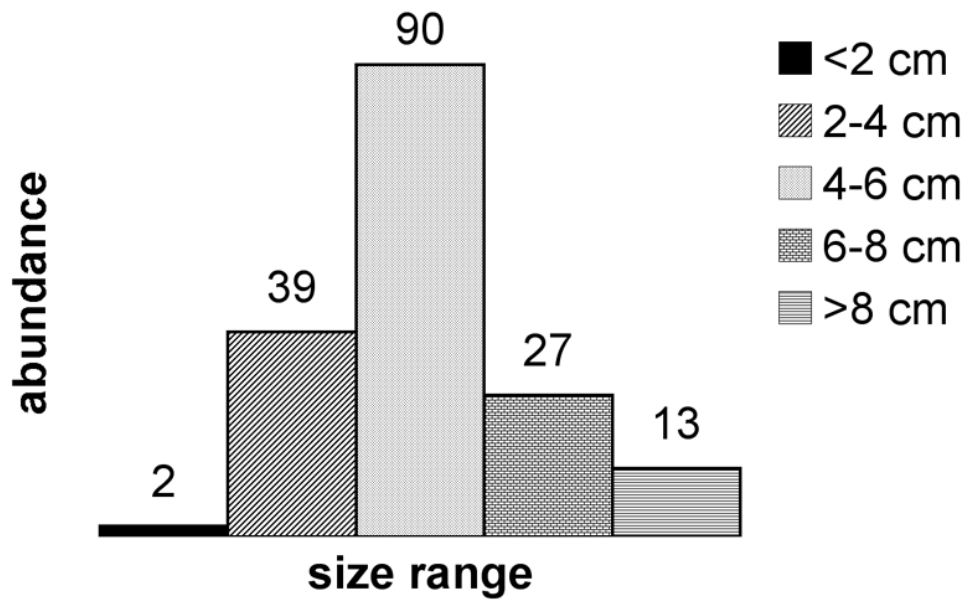


Fig. 1



**Fig 2**



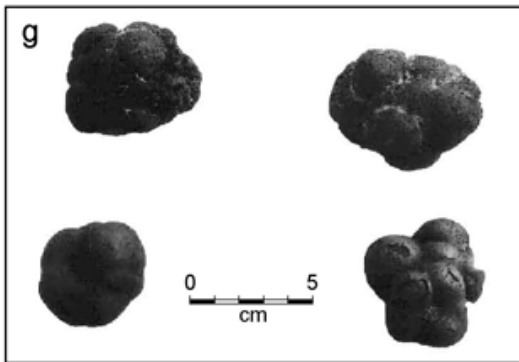
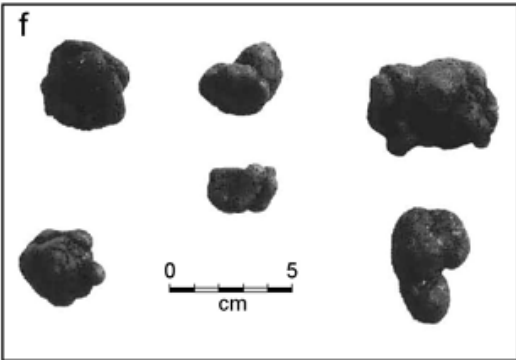
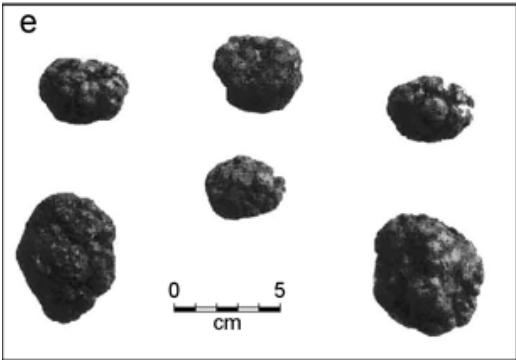
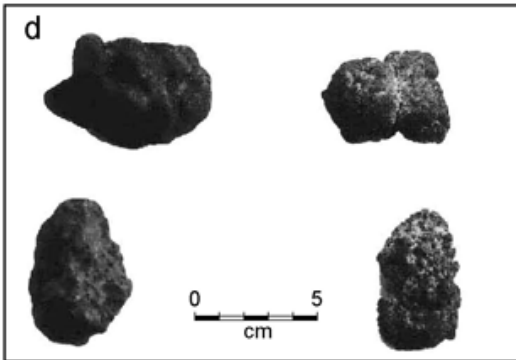
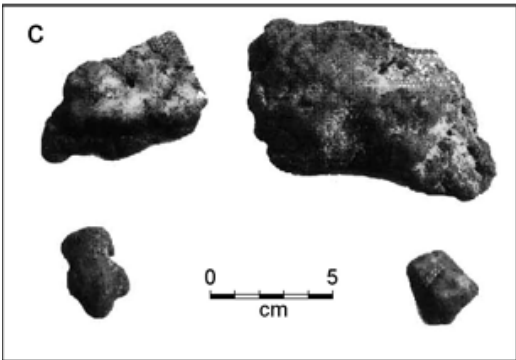
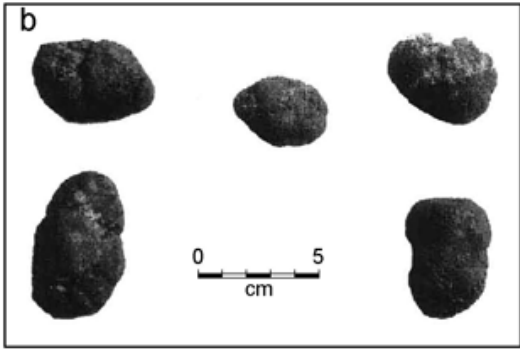
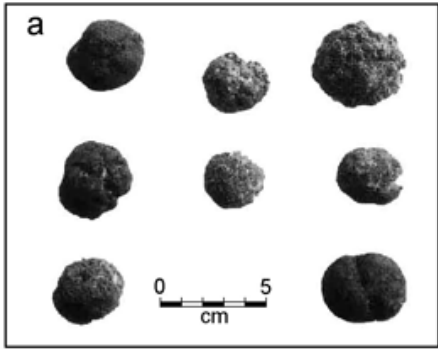


Fig. 3

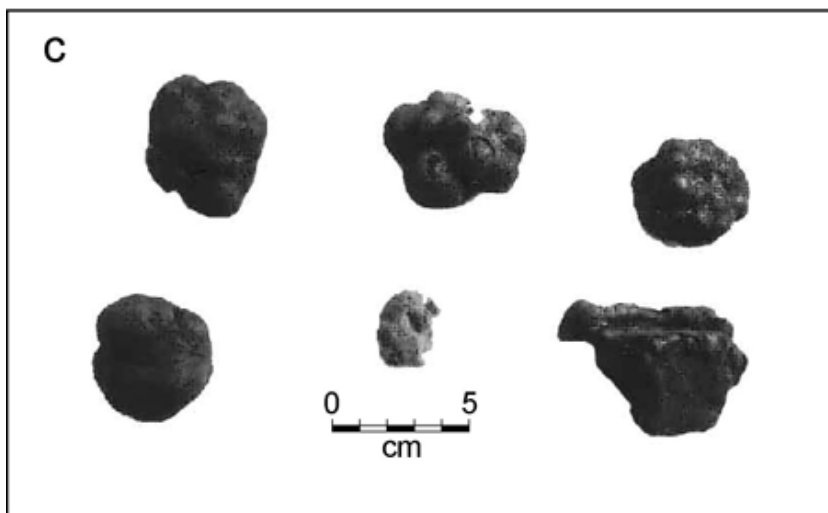
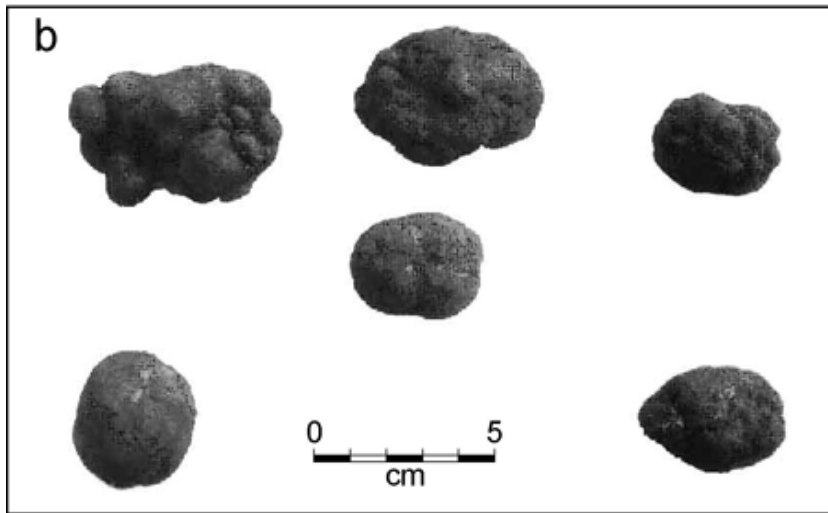
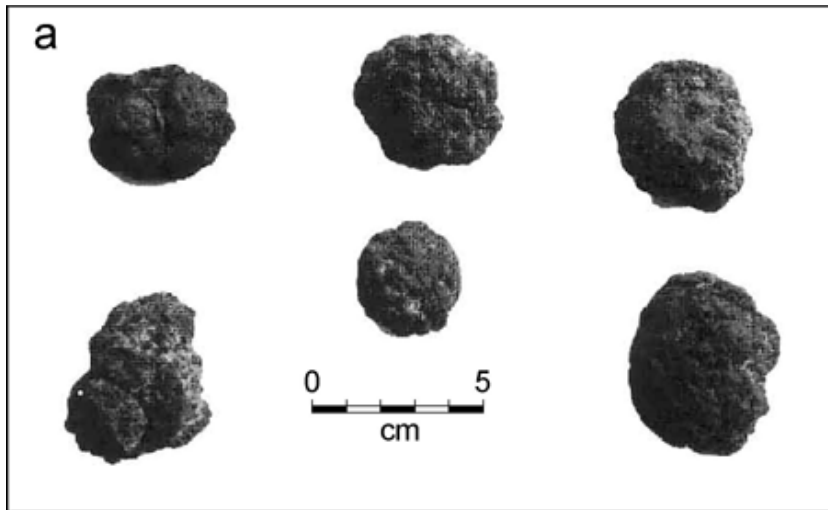
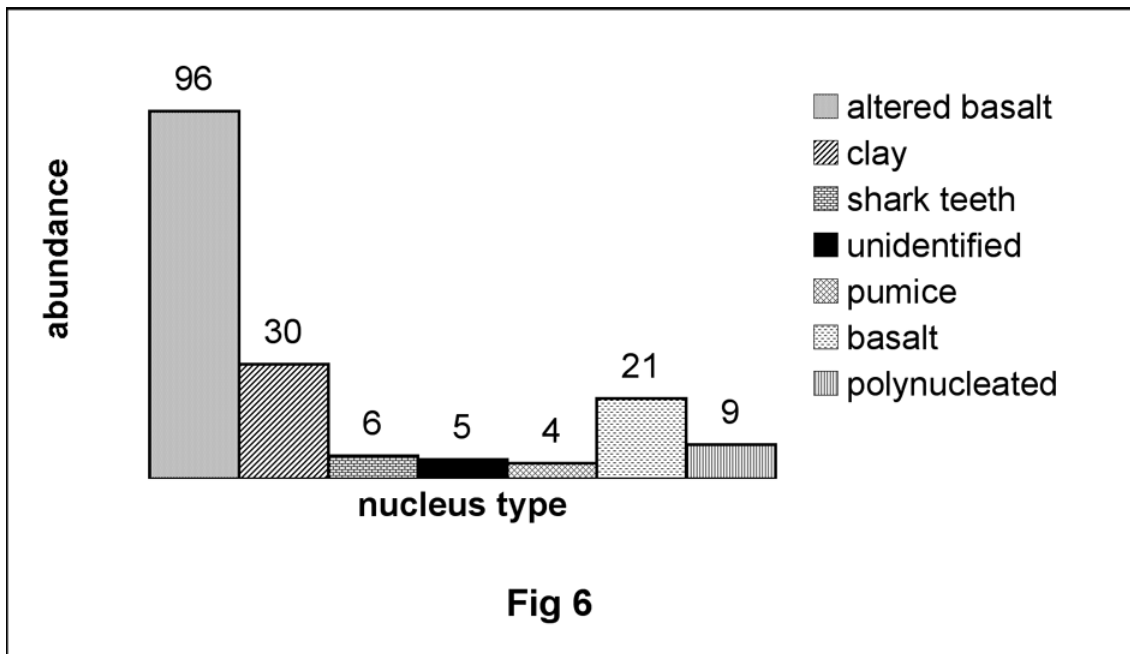
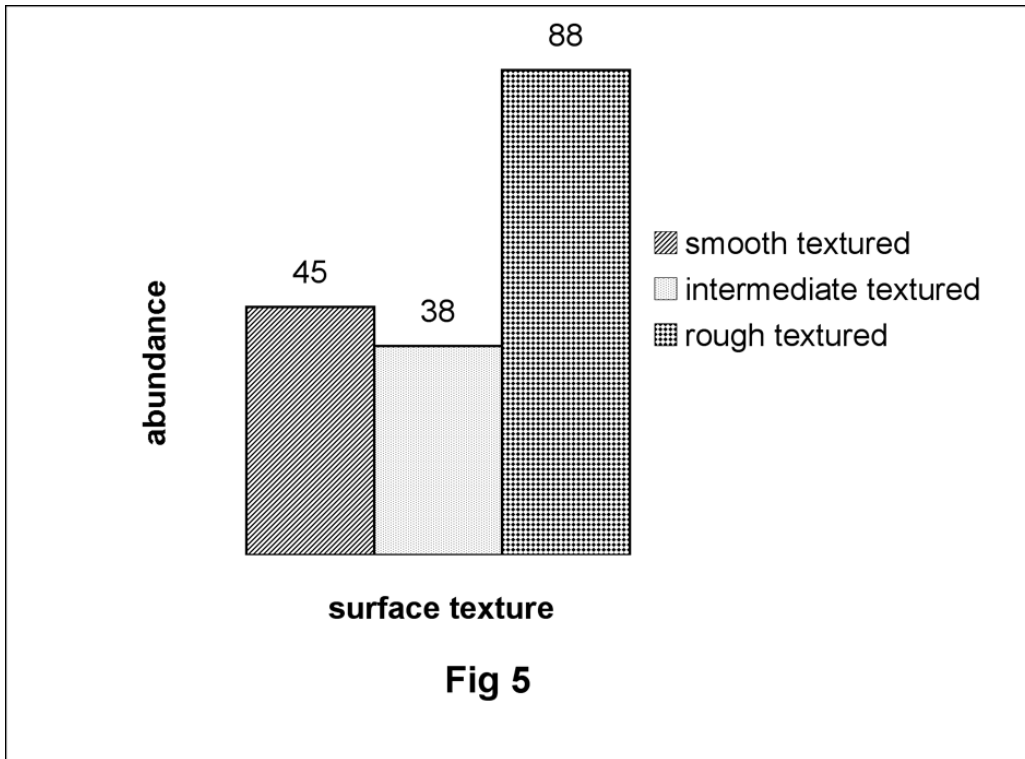


Fig. 4



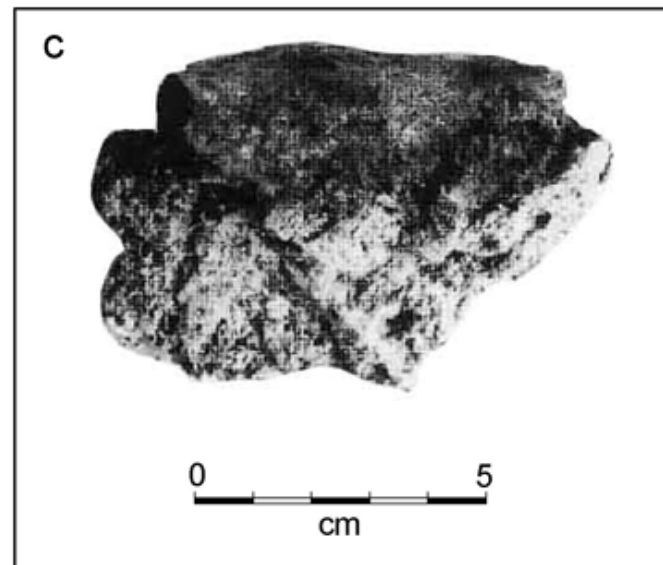
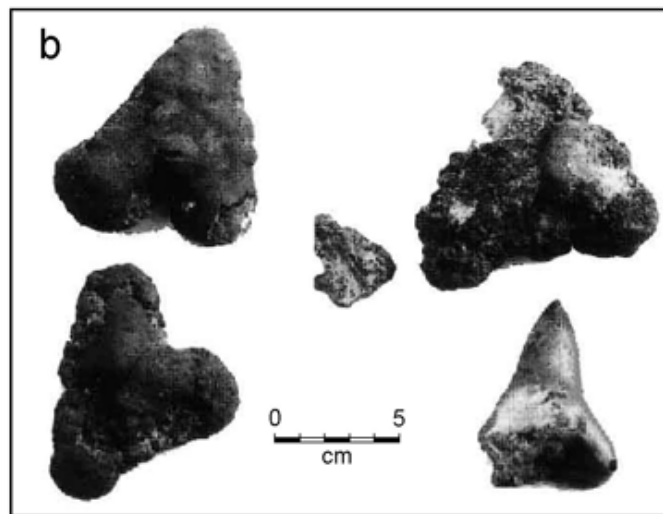
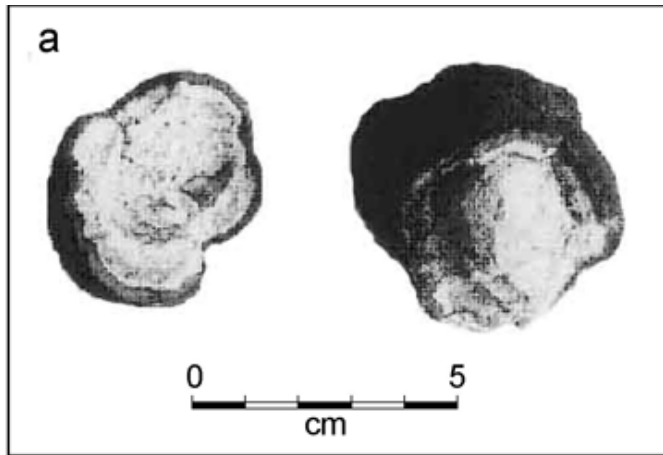


Fig. 7

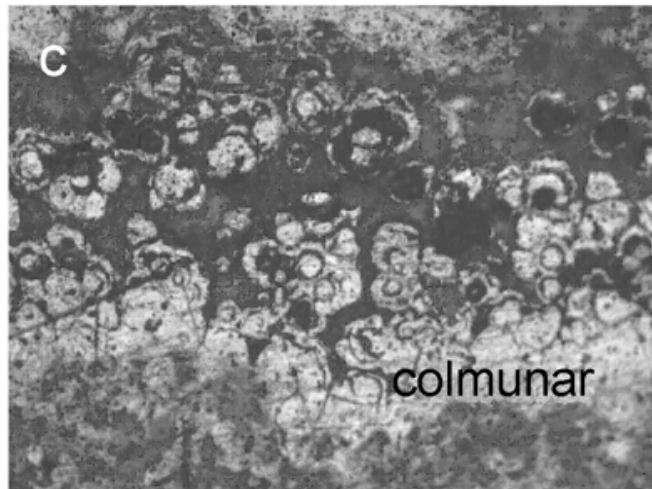
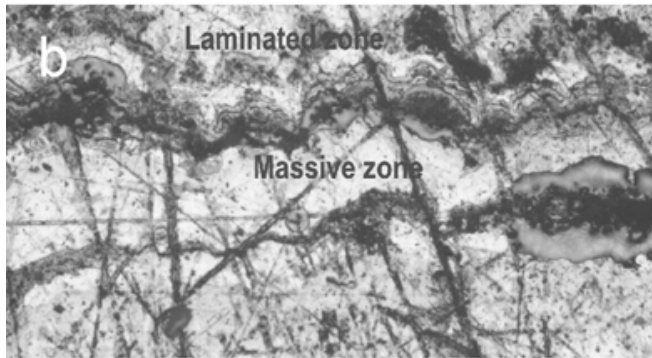
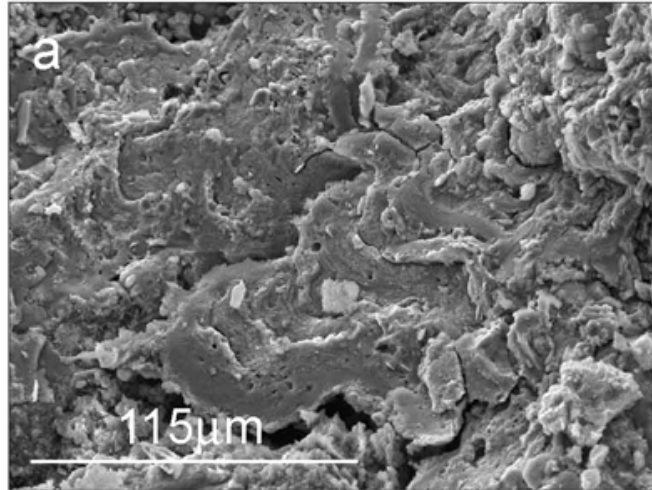


Fig. 8

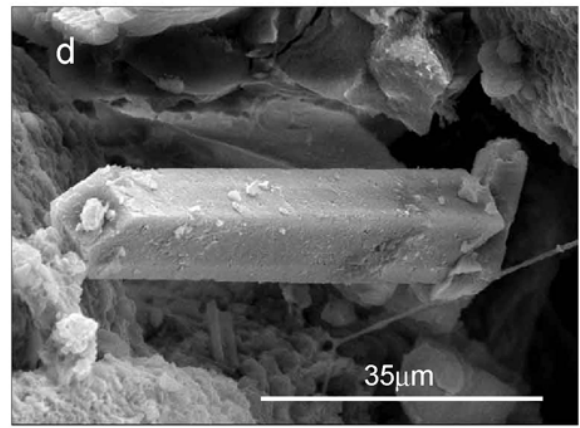
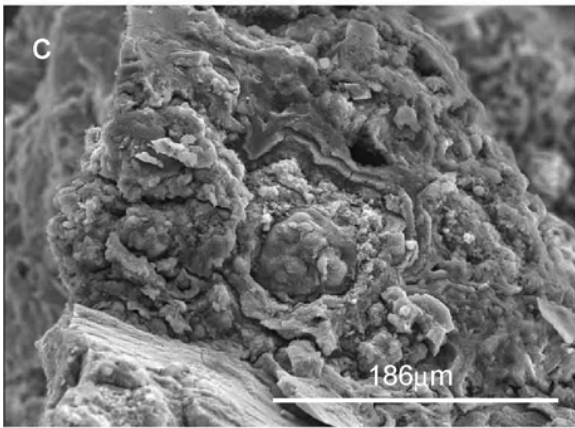
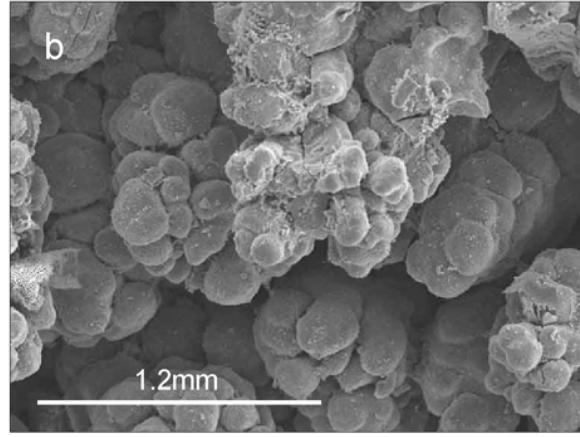
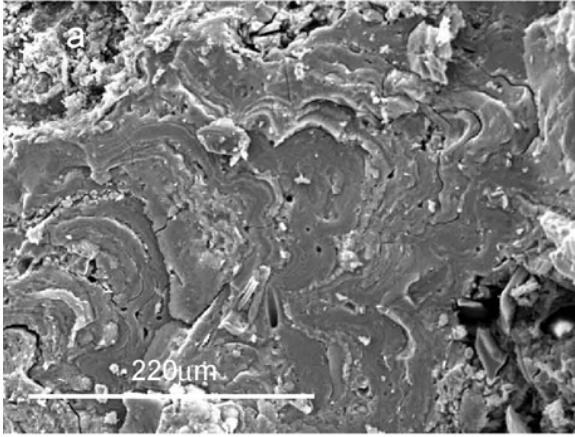


Fig. 9

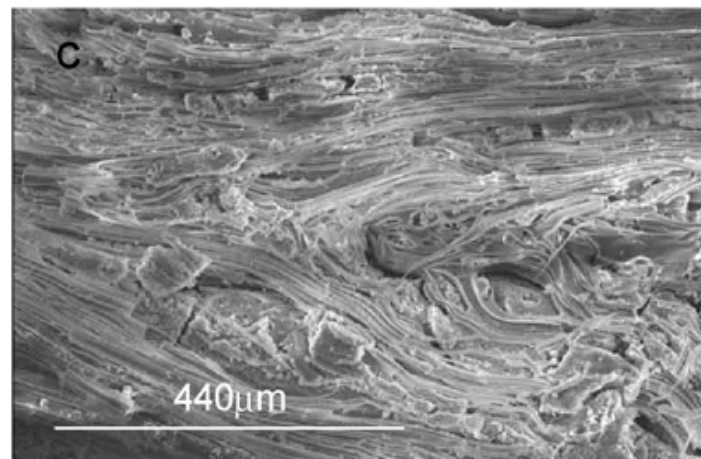
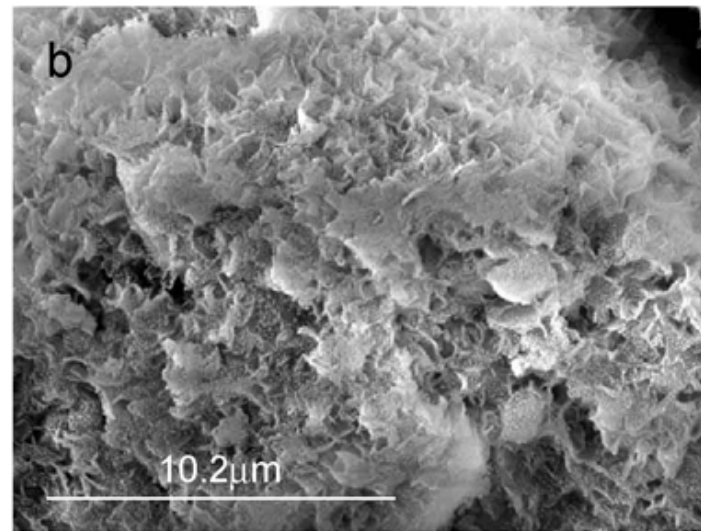
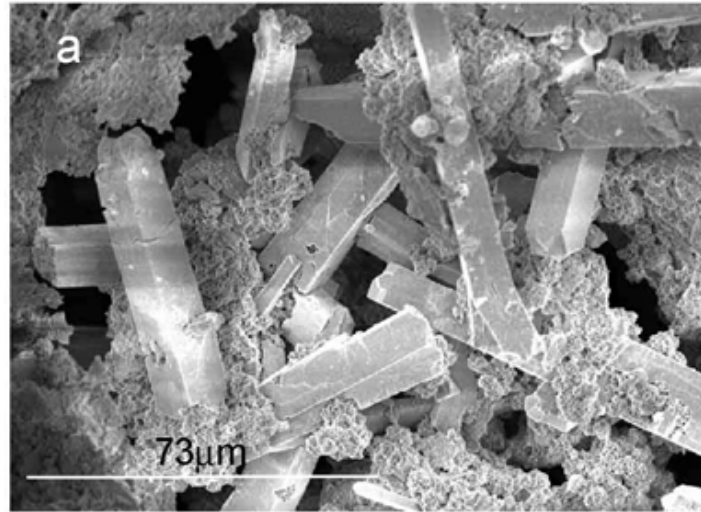


Fig. 10

Table 1

Serial No	Cruise no	Sample no	Latitude (°S)	Longitude (°E)	Type of sampler	Water depth (m)	Nodule abundance (kg/m <sup>2</sup> )
1	SKA002	0129C	12.0020	76.4470	Freefall grab	5100	14.46
2	SKA003	0167G	11.5000	75.5000	Freefall grab	na	08.46
3	SKA003	0193F	12.5190	80.9510	Freefall grab	4860	13.85
4	SKA003	0190A	12.5060	79.4760	Photograb	5112	00.77
5	SKA003	0190B	12.5060	79.4760	Freefall grab	5112	01.38
6	SKA003	0190C	12.5060	79.4760	Freefall grab	5112	00.92
7	SKA003	0190D	12.5060	79.4760	Freefall grab	5112	01.54
8	SKA003	0190E	12.5060	79.4760	Freefall grab	5112	03.23
9	SKA003	0190F	12.5060	79.4760	Freefall grab	5112	na
10	SKA003	0184G	14.0200	79.3960	Freefall grab	5172	11.53
11	SKA004	0280F	11.9920	76.4840	Freefall grab	5400	06.23
12	SKA005	0351B	11.2590	74.0010	Photograb	5061	02.38
13	SKA006	0372E	10.9790	77.8710	Dredge	5300	na
14	SKA006	0372J	11.0890	77.8390	Dredge	5300	na
15	SKA006	0423B	11.2500	82.5000	Freefall grab	5050	04.92
16	SKA006	0374E	11.7460	76.9980	Dredge	5400	na
17	SKA008	0506A	10.7510	83.5000	Freefall grab	5250	15.38
18	SKA008	0521B	13.7480	78.9990	Freefall grab	5100	13.69
19	SKA009	0592C	13.5010	77.1200	Photograb	5400	03.85
20	SKA009	0557C	14.5010	75.1200	Freefall grab	5140	11.54
21	SKA009	0552A	14.3740	75.2330	Freefall grab	5210	13.46
22	SKA010	0653C	13.6130	76.0730	Dredge	5300	na
23	SKA010	0650G	12.4670	76.8670	Dredge	na	na
24	SKA011	0669H	12.4940	76.7530	Dredge	5520	na
25	SKA011	0664L	12.5870	76.1010	Dredge	5250	na
26	SKA011	0670J	12.7250	75.8060	Dredge	5250	na



Serial No	Cruise no	Sample no	Latitude (°S)	Longitude (°E)	Type of sampler	Water depth (m)	Nodule abundance (kg/m <sup>2</sup> )
27	SKA011	0665A	12.4980	76.1330	Dredge	5350	na
28	SKA011	0663W	12.5780	76.0690	Dredge	5250	na
29	SKA013	0699	12.9980	76.9970	Dredge	5430	na
30	SKA014	0716A	12.0010	75.8710	Freefall grab	5230	06.92
31	SKA014	0716C	12.0000	75.8670	Freefall grab	5230	na
32	SKA014	0721B	12.7470	75.6190	Photograb	5140	17.73
33	SKA015	0762A	11.5020	75.3710	Photograb	na	02.65
34	SKA015	0781D	11.3800	73.4960	Freefall grab	na	15.35
35	SKA016	0790B	10.8740	73.8780	Freefall grab	5250	15.58
36	SKA016	0814C	13.4950	74.4970	Freefall grab	5325	14.00
37	SKA016	0823C	13.7510	74.1230	Freefall grab	5340	01.31
38	GAR001	0009C	11.8770	76.2470	Photograb	5320	10.15
39	GAR003	0112C	11.8750	75.6280	Photograb	5210	03.96
40	GAR003	0121A	12.3830	76.2140	Dredge	5220	na
41	GAR003	0123F	12.6370	76.3690	Dredge	5000	na
42	FAR001	0005A	10.4990	74.5010	Freefall grab	4581	08.46
43	FAR001	0055B	14.9980	72.5030	Freefall grab	4500	14.62
44	FAR001	0061D	14.0000	75.5010	Freefall grab	5091	02.92
45	FAR002	0088B	12.7480	76.9980	Freefall grab	5496	na
46	FAR002	0088C	12.7480	76.9990	Freefall grab	5503	07.69
47	FAR002	0095C	11.9860	76.5160	Dredge	5402	na
48	FAR003	0109A	10.6580	74.8050	Freefall grab	5175	00.89
49	FAR003	0122D	11.2620	77.0180	Freefall grab	5380	00.77
50	FAR003	0142C	08.4680	81.5090	Freefall grab	na	08.46
51	FAR004	0198A	11.546	79.921	Freefall grab	na	na
52	FAR005	0210A	13.2470	74.4980	Freefall grab	5200	10.92
53	FAR005	0228E	11.7500	78.2490	Freefall grab	5410	03.23
54	FAR005	0235D	14.0040	76.7480	Freefall grab	5210	03.80
55	SKY007	0043F	15.2680	75.9600	Freefall grab	5075	16.92

Serial No	Cruise no	Sample no	Latitude (°S)	Longitude (°E)	Type of sampler	Water depth (m)	Nodule abundance (kg/m <sup>2</sup> )
56	NR0001	0022C	11.1220	78.3660	Freefall grab	5175	14.62
57	NR0001	0047C	12.2500	78.3690	Freefall grab	5425	16.15
58	NR0002	0083A	13.3710	79.0010	Freefall grab	5400	00.77
59	NR0002	0083B	13.3740	79.0000	Freefall grab	5400	05.38
60	NR0003	0128E	10.6300	75.3520	Freefall grab	5200	17.69
61	NR0004	0158B	11.0010	73.3790	Freefall grab	5075	12.31
62	NR0004	0158C	11.0010	73.3790	Freefall grab	5075	13.85
63	AAS014	0088A	14.8740	75.2580	Okean grab	5080	05.20
64	AAS014	0088B	14.8420	75.2480	Okean grab	4999	02.80
65	AAS038	0263	11.6236	78.8096	Okean grab	na	09.60

na- not available

Legend: Research Vessels: SKA- Skandi Surveyor; GAR- G A Reay; FAR- Farnella;  
NR- Nand Rachit; AAS-A A Sidorenko

Table 2.

Sl no	Sample no	Size (cm)	Type of nucleus	Shape	Surface texture	Remarks
1	SS2/87B	6-7	altered basalt	rounded, sub-rounded, elongated, discoidal	rough	mostly single nucleus, some polynucleated.
2	SS2/74C	4	altered basalt	bean shaped	smooth	mostly broken into small chips, mammilated
3	SS2/92A	7.2		rounded, triangular, botryoidal	smooth	botryoids on rough surface
4	SS2/90B	<2	altered basalt	discoidal	smooth	may be a piece of crust, shieve like thing
5	SS2/86DRDG	6.1		potato shaped	rough	some polynucleated
6	SS2/120 ABCD	6.2	pumice	hamburger type	rough	mostly pumice, very few nodules polynucleated, extremely flat shaped, mammilated
7	SS2/122C	7-7.5	altered basalt	disc shaped	smooth to intermediate	
8	SS2/107A	4.5	altered basalt	sub-rounded	rough	fragile, some infilled with sediment
9	SS2/110c	4.5	basalt	potato shaped	smooth	very fragile
10	SS2/129C	7.1		elongated, triangular	rough	clay on surface, hard to break.
11	SS3/162D	5.8		spheroidal	rough	extremely fragile
12	SS3/134F	5.5	altered basalt	ellipsoidal	rough	hard to break
13	NR3/128E	6.5	altered basalt	polynucleated	smooth	clay on surface, mammilated
14	NR3/126B	5.3		irregular	intermediate	mammilated
15	NR3/126E	3.7		polynucleated	rough	mammilated
16	NR3/126E	4.9		potato shaped	rough	vitreous luster
17	NR2/90E	4	basalt	ellipsoidal	intermediate	a brown spot at the rim
18	NR2/101C	4		sub-rounded	intermediate	
19	NR4/158D	70 % < 3	basalt, pumice	mostly polynucleated	smooth	extremely mammilated growth
20	NR4/158BC	2-4, one of 9.1	altered basalt	rhombic shaped, multystoried	intermediate	
21	SS3/167G	5	palagonite	sub-rounded to elipsoidal	rough	
22	SS3/157C	4.8	altered basalt	ellipsoidal	intermediate	
23	ss3?167c	80 % < 6		pitted, irregular	very rough	clay coating
24	SS3/147G	2-4, 6.1	altered basalt	irregular, discoidal	intermediate	mammilated
25	SS3/137G	200, 2-4	altered basalt	small irregular	smooth	
26	NR2/101AB	various size, 6	basalt	sub-rounded to grounded	rough	
27	NR4/158D	5		irregular	smooth	mammilated
28	NR1/22C	7.1	altered basalt	irregular, botryoidal	intermediate	mammilated
29	NR3/128A	7.9	basalt	botryoidal, ellipsoidal	smooth	shiny surface, biogenic growth
30	NR1/47C	up to 11		hamburger type	rough	may be shark tooth inside

Sl no	Sample no	Size (cm)	Type of nucleus	Shape	Surface texture	Remarks
31	NR2/71D	up to 3.8		discoidal	smooth	
32	NR2/69DE	up to 5.6		sub-rounded	very rough	sediment in pore space
33	NR2/83AB	up to 6	clay palagonite	discoidal, sub-rounded	very rough	clay within nucleus yellow mineral in core and flat shaped.
34	SS3/182AG	70 % < 3.4	yellow min.	mainly disc like	rough	highly coated with sediment
35	AAS3/ B15/55	7.3	altered basalt	ellipsoidal, flatbottom	very rough	surface alteration, mammilated
36	SS3186/H	small size	altered basalt	potato shaped, ellipsodal	sooth, brownish colour	small nodules plenty, mammilated
37	SS3/193F	3		rough	smooth, brownish colour	maximum broken nodules
38	SS3/191F	4.6		triangular	smooth	ridge like feature, mammilated
39	SS3/184G	6		largely irregular	intermediate	all are almost equal size, hard
40	SS3/190ABCDEG	2.5		rounded	very rough	broken fragments plenty sediment in pore space , hard to break
41	SS4/237D	small pieces	altered basalt	small tadpole shape	Smooth	small fragments
42	SS4/216B	some < 4.5		dumb bell	gritty rough	clay covered
43	SS4/228E	small chips	altered basalt	small chips	intermediate to smooth	nucleus is eccentrically located
44	SS4/250E	small up to 2.6	altered basalt	Irregular	smooth	some encrustations with nodules
45	SS4/254G	4.1	altered basalt	discoidal, irregular, ellipsoid	intermediate	small nodule
46	SS4/270ABCEG	small pieces	altered basalt	small broken ones	smooth	small pieces
47	SS4/280F	mostly up to 4	altered basalt	irregular	gritty rough	large nucleus, mammilated
48	SS4/280Q	similar size 4.8	altered basalt	ellipsoidal, potato shaped	gritty rough	all of similar size
49	SS5/311C	5.6	large nucleus	sub-rounded	intermediate	?shiny mineral in nucleus
50	SS5/301H	similar size 4		rounded to ellipsoidal	rough	rough, blistering
51	SS5/309ABC	variable	altered basalt	ellipsoidal, discoidal	rough to intermediate	a few large samples, sediment on surface
52	SS5/330ACDE	7		irregular	rough, blistering	most specimens of same size
53	SS5/351B	6.3		rectangular	very rough	?shiny mineral in nucleus
54	SS6/372J	85 % up to 3.5		highly rounded	rough	several specimens have rounded nucleus
55	SS6/372E	4		rounded	rough	all are similar looking
56	SS6/374E	4	altered basalt	ellipsoidal, sub-rounded	knobby	all with pumice nucleus
57	SS6/390D	90 % up to 3.6, one of 10	pumice, basalt	ellipsoidal	intermediate	
58	SS6/404D	4-6 various size up to 10	basalt	irregular	smooth	
59	SS6/423B	10	pumice	rhombic, discoidal	smooth with some botryoids	
60	SS8/521B	2-4	basalt	small irregular	smooth	
61	SS8/511D	6.2		irregular	intermediate	very hard to break, mammilated

SI no	Sample no	Size (cm)	Type of nucleus	Shape	Surface texture	Remarks
62	SS8/506A	90 % small up to 5.2	basalt	triangular	intermediate to smooth	90% specimens are broken or very small
63	SS8/540all	small pieces	basalt	irregular	intermediate	all of same shape and size
64	SS7/463E	3.9		ellipsoidal	smooth	several broken pieces
65	SS9/552A	5.7	basalt	irregular shaped	intermediate	
66	SS9/568ABC	2.7		sub-rounded to rounded	gritty rough	
67	SS9/569AB	4, one 6.8		irregular, botryoidal	rough	mammilated
68	SS9/559AB	60 % small		irregular	rough to intermediate	mammilated
69	SS9/557C	same size 4	altered basalt	nodular, potato shaped	intermediate	
70	SS9/556AB	4.7	altered basalt	discoidal, ellipsoidal, one side	rough	mammilated
71	SS9/600C	8.5	altered basalt	Irregular shaped	rough	large nucleus
72	SS9/597B	90 % up to 4.8, 6.5		irregular	very rough	2 distinct size modes
73	SS9/603A	4	altered basalt	polynucleated	smooth to intermediate	sediment covered
74	SS9/592C	13		oval	smooth to intermediate	large nucleus, sediment covered
75	SS9/647B	6	altered basalt	potato shaped	rough	one side rougher than other surface
76	SS9/619C10	10		subrounded	rough	sediment on surface
77	SS9/618B	mostly 4		sub-rounded	rough	fish tooth
78	SS9/621C	broken, one of 13	shark teeth	irregular, triangular	rough	sediment, large tooth of a shark
79	SS9/624AB	90 % 2-4	altered basalt	ellipsoidal	rough	
80	SS9/638B	small chips	altered basalt	small chips	smooth	broken pieces
81	SS9/644B	chips <1 cm		small chips	smooth	broken fragments
82	SS10/655B	2-4		rounded, ellipsoidal	rough	all similar shaped, highly sediment covered
83	SS10/650G	variable	basalt, pumice	irregular	rough	partly coated rock
84	SS10/nod from prev cruise	70 % large		ellipsoidal	rough	sediment infill
85	SS10/657 spade core	60 % <2.3	altered basalt	irregular	intermediate	mammilated
86	SS10/653C	70 % <4.6	pumice	elongated, triangular	rough	coated pumice????
87	SS11/663W	90 % <2.3	basalt	large = irregular, small = ellipsoidal	rough on one side	sediment filled
88	SS11/664C	2 large 10, 8	basalt	rough	intermediate	sediment filled, mammilated
89	SS11/664L	10	pumice	flat, triangular	rough	pumice, altered basalt
90	SS11/665A	variable	pumice, shark's teeth	irregular	rough	shark's teeth, pumice
91	SS11/670J	2-4		flat bottom	very rough	
92	SS11/669H	variable	altered rock	irregular	intermediate	partly coated rock

SI no	Sample no	Size (cm)	Type of nucleus	Shape	Surface texture	Remarks
93	SS14/716AC	2-4		ellipsoidal, rounded	gritty	variable roughness
94	SS11/665A	encrustations			one gritty, other smooth	Encrustation
95	SS13/682	variable		sausage type	very earthy	
96	SS13/684	variable	shark teeth	triangular	intermediate	shark's teeth
97	SS13/691A	90 % 2-4		rounded, ellipsoidal	gritty	
98	SS13/692B	60 % 2-4		rounded, ellipsoidal	gritty	surface very muddy
99	SS13/699	variable		triangular, disc	gritty to smooth	
100	SS13/704B	variable	shark's teeth	triangular	very gritty, knobby	
101	SS14/717A	70 % small		rounded	grainy	one surface smooth, botryoidal other is rough
102	SS14/721B	50 % broken		elongated, discoidal	smooth to intermediate	
103	SS14/733D	80 % small		sub-rounded, elongated	smooth	
104	SS14/710C	80 % small	altered basalt	small = rounded, large = elongated	smooth	
105	SS15/753B	4-6		sub-rounded, elongated	very gritty, knobby	sediment infilled
106	SS15/743A	4-6		discoidal	gritty	all same shape, sediment covered
107	SS15/767	broken pieces	altered basalt	chips	intermediate	broken fragments
108	SS14/708BCEG	4-6		rounded	very rough	sediment covered
109	SS15/769D	90 % small		rounded	intermediate	
110	SS15/766A	80 % large		rough	intermediate	larger have sediments, mammilated shark's teeth and basalt within same nodule, mammilated
111	SS15/771A	80 % large		rough	smooth	
112	SS15/762A	40 % small		irregular, botryoidal	very rough	surface clayey
113	SS15/778E	fragments	altered basalt	irregular	smooth	
114	SS15/783A	4-6		sub-rounded	smooth	
115	SS15/776E	90 % < 1		irregular	intermediate	abundance of micronodules
116	SS15/776D	variable		flat, botryoidal	smooth	encrustations and nodules
117	SS15/781D	70 % small	altered basalt	disc type	smooth	shiny face, mammilated
118	SS16/838C	90 % small		discoidal	intermediate	
119	SS16/789F	variable		sub-rounded	very gritty	sediment covered
120	SS16/808F	2-4		irregular shaped, crust polygonal	gritty	one encrustation
121	SS16/790B	variable		rough	one gritty, other smooth	mammilated
122	SS16/814C	variable	shark's teeth	triangular	one gritty, other smooth	shark's teeth
123	SS16/809A	2-4	altered basalt	irregular	smooth	polished appearance
124	SS16/823C	50 % small	pumice, basalt	rough	partially covered pumice	
125	SS16/820G	variable		flat chip like	rough	
126	SS16/838D	2-4			intermediate	polished appearance

SI no	Sample no	Size (cm)	Type of nucleus	Shape	Surface texture	Remarks
127	SS16/826E	2-4		potato shaped, ellipsoidal	smooth	polished appearance
128	SS16/828E	90 % small		smooth	smooth	polished appearance
129	F2/88	2-4		ellipsoidal, sub-rounded	gritty	sediment covered
130	F296F	variable		irregular, ellipsoidal	uneven	sediment covered
131	F1/5A	2-4	shark's teeth	elongated, rounded	very gritty	sediment covered
132	F1/4DRDG	70 % small		irregular	gritty	
133	F1/18A	small > 4.5		irregular	gritty	sediment covered
134	F1/17A	90 % small		irregular	smooth	mammilated
135	F1/23A	max broken	altered basalt	irregular	smooth	mammilated
136	F1/37B	70 %, small		small = rounded, large = elongated	very rough	sediment covered
137	F1/44C	small broken	altered basalt	broken chips	intermediate	mostly broken
138	F1/46E	all broken	altered basalt	flat bottomed	gritty to smooth	
139	F1/58D	all broken			variable	
140	F1/61D	90 % small		discoidal, ellipsoidal	gritty to smooth	sediment covered
141	F1/55B	all broken	altered basalt	various shaped	gritty to smooth	sediment covered
142	F1/60D	2-4		ellipsoidal	gritty to intermediate	mammilated
143	F2/79C	2-4		ellipsoidal, flatbottom	gritty to smooth	sediment covered
144	F2/80B	variable	palagonite	angular	intermediate	partially encrusted
145	F2/73 D	2-4		large = triangular, small = elongated	gritty to smooth	sediment on rough surface
146	F2/74B	90 % smaller		small = rounded, large = elongated	intermediate	very rounded shape
147	F2/88BC	2-4		rounded to sub-rounded	gritty	
148	F2/95C	broken, 1 crust		small broken ones	upper surface very rough	
149	F2/95D	70 % small		rough	intermediate	mammilated
150	F2/97F	variable	pumice, basalt	nodular, potato shaped	rough	mostly covered pumice
151	F3/122D	variable		potato shaped	very loose, gritty	sediment covered
152	F2/84E	90 % <2	altered basalt	irregular	smooth and shiny	
153	F2/109A	variable	shark's teeth	triangular	very rough	shark's teeth, sediment
154	F3/103D	90 % very small		irregular shaped	very rough	sediment on very rough surface
155	F3/124CD	mostly large			rough	sediment coated, mammilated
156	F3/125A	70 % >6	altered basalt	irregular	intermediate	sediment on side, mammilated
157	F3/133ACD	2-4		ellipsoidal	rough	
158	F3/142C	2 size modes		ellipsoidal	smooth	
159	F3/174BCD	variable		sub-rounded	very rough	sediment covered
160	F4/198	70 % smaller	pumice, basalt	rounded to elongated	rough	2 types of nucleus
161	F4173A	80 % large		irregular, botryoidal	very rough	

SI no	Sample no	Size (cm)	Type of nucleus	Shape	Surface texture	Remarks
162	F5/210A	variable		flat bottom	smooth	brownish surface
163	F5/228E	2-4		potato shaped	gritty and fragile	
164	F5/235D	80 % <2	shark's teeth	triangular and ellipsoidal	rough	sediment, shark's teeth
165	F5/244C	70 % <3.5		ellipsoidal	rough	sediment coated
166	F5/238A	60 % <2		elongated, rounded	rough to intermediate	
167	F6/274B	2-4		uneven	very rough	sediment coated, mammilated
168	F6/303BH	small pieces	basalt	various small chips	smooth	
169	F6/288B	all same but 3		various shaped	smooth	
170	F6/302B	80 % 3-4	altered basalt	mostly rounded	intermediate	
171	F6/264A	2-4		elongated	very rough	sediment coated
172	F7/328C	80 % broken		irregular	smooth	broken nodules, mammilated
173	F7/356G	2-4e		uneven	smooth	mammilated
174	F7/374A	2-4		squarish, ellipsoidal	intermediate	
175	F7/353E	3-4 cm		uneven	rough	mammilated
176	F7/344E	70 % broken	altered basalt	variable	smooth	mostly broken nodules
177	F8/389G	70 % broken	altered basalt shark's teeth, basalt	variable	smooth	mostly broken nodules
178	F8/123A*H	variable		rounded	intermediate	shark's teeth
179	F8/397ABC	80 % broken	clayey	rounded	smooth to intermediate	
180	F8/399EF	80 % broken		variable	smooth to intermediate	broken nodules
181	GR1/9C	80 % small, crust		crust = sheet like, nodule = elongated	rough	encrustation and nodule
182	GR1/23B	70 % small		rounded to elongated	rough	few with sediment coating
183	Gr1/13D	2-4		sub-rounded, elongated	very rough	mammilated
184	GR1/11A	max <6, few >6		sub-rounded, pancake like	very rough	shark tooth inside
185	F8/398E	80 % <3-4	altered basalt	various shape	Smooth	weathered
186	GR3/129B	2-4		flat bottom	very rough	sediment coated
187	GR3/1213F	4-6	shark's teeth	chunk like	very rough	encrustation, shark tooth
188	GR3/121A	2-4	clay, palagonite	uneven	smooth	polished surface
189	GR3/99C	2-4		one encrustation	rough	sediment coated, mammilated
190	GR3/131D	2-4		rounded	rough	mammilated
191	GR3/112C	80 % 2-4		rounded	very rough	
192	SK6/4B	variable		rounded, ellipsoidal	very gritty	sediment coated
193	SK6/7E	one >7 rest small		rounded, ellipsoidal	very rough	sediment coated
194	SK6/11all	70 % broken	altered basalt	uneven	smooth	mammilated
195	SK7/22C	small broken	altered basalt	irregular, botryoidal	smooth to intermediate	
196	SK7/43F	80 % small l<3	clay, palagonite	variable	gritty to smooth	mammilated



Sl no	Sample no	Size (cm)	Type of nucleus	Shape	Surface texture	Remarks
197	SK7/46EF	2-4		rounded, sub-rounded	intermediate	
198	SK7/50ACDF	2-4		pancake shaped	very rough	sediment coated
199	SK8/61B	80 % small, 2 big		ellipsoidal, small = rounded	smooth to intermediate	
200	AAS26/DR25	70 % small 2-3		small = rounded, large = elongated	intermediate	
201	AAS24/D23	80 % small, crust		rounded to sub-rounded, crust = flat	rough	encrustation
202	SK11/100AFD	3 - 4		rounded	intermediate	
203	SK11/126E	chips <1		very small fragments		broken fragments
204	SK11/145BD	30 % 2-4		irregular	rough to intermediate	broken nodules
205	AAS17/135	2-4		elongated	very rough	sediment covered
206	AAS14/88AB	70 % 2-4		uneven	rough to intermediate	mammilated
207	AAS36/177	2-4		irregular, discoidal	gritty to smooth	upper surface very smooth
208	AAS37/263[2/2]	2-4		irregular	intermediate	sediment coated

Table 3.

Sl no	Sample no	L (cm)	W (cm)	T (cm)	Oxide thickness (mm)	Av oxide thickness (cm)	Nucleus thickness (cm)	Ratio of nucleus to oxide	Type of nucleus
1	AAS2/D23 NOD	3.8	3.5	2.8	5+7+3	0.5	1.3	2.6	AB
2	AAS2/D23 CRUST	7.7	5.5	1.6	very thin	very thin	1.2		AB
3	SK11/145BD	3.1	2.1	1.4	2+2+1	0.167	1	5.99	AB
4	AAS14/88AB	4.2	3.6	3	3+2+3	0.267	1.1	4.12	AB
5	AAS36/#177	5.7	4.7	3.2	4+4+5	0.433	1.4	3.23	C
6	AAS17/135	4	3.6	3.8	8+3+6	0.567	.4,.7	1.03	AB
7	F8/123A*H	4.3	4	4	3+3+5	0.367	0.9	2.45	ST
8	F1/55B	2	1.5	0.9					U
9	F3/122D	4.6	3.8	3.2	8+5+6	0.633	0.8	1.26	C
10	F3/174BCD	5.9	5.8	3.7			0.9		C
11	SK7/22C	3.3	2.3	2.6	2+2+1	0.167	1.7	10.18	AB
12	F5/244C	6.1	3.5	3.7	8+6+2	0.533	0.7	1.31	C
13	F1/5A	4.7	3	2.8	6+3+4	0.433	1.2	2.77	MIXED
14	AAS37/#263	6	4.3	4.4	11+7+4	0.733	2.3	3.14	C
15	F5/235D	4.6	3.7	2.2					ST
16	F4/374A	4.3	4	2.7	7+5+6	0.6	0.6	1	C
17	F5/238A	5.1	3.2	2.5	2+3+3	0.267	0.8	2.99	AB
18	F6/302A	4.9	3.3	3.1	3+3+3	0.3	0.9	3	AB
19	F5/210A	4.8	3.3	2.2	7+5+3	0.5	0.5	1	AB
20	SK7/46EF	3.1	3	2.1					AB
21	AAS26/DR25	4.3	4	3.6	4+3+5	0.4	1.8	4.5	AB
22	SK8/50ACDF	5.2	4.1	3.3	3+2+1	0.2	2	10	AB
23	SK8/61B	7.5	4.6	3.3	6+4+3	0.433	1.7,1.2	0.29	AB
24	F8/398E	4.3	3.4	3.4	3+2+2	0.233	1.6,.5	0.22	AB
25	SK7/43F	5.4	4	2.9	22+3+1	0.2	1.4	7	AB
26	F7/328C	3	2.3	1.9					AB
27	F8/397ABC	3.4	3.3	2.1	1+2+2	0.167	0.9	5.39	AB
28	F6/264A	4.2	3.8	2.6	3+3+1	0.233	.6,.4	0.47	AB
29	F5/228E	3.8	3.3	2.3	7+7+7	0.7	0.6	0.86	AB
30	F3/133ACD	5.2	3.8	3.5	5+11+4	0.667	1.2	1.80	AB
31	F4/198	3.8	3.6	2	1+2+1	0.133	1.7	12.78	P
32	F3/142C	5.5	3.7	2.7	3+2+3	0.267	1.7	6.37	AB
33	F3/124CD	9.7	7.6	6.6					AB
34	F3/109A	5.9	4.1	3.4	6+4+6	0.533	1.3	2.44	AB
35	SK6/4B	5.5	3.7	2.9	7+2+5	0.467	1.2	2.57	AB
36	F7/356G	4.8	4.7	3.7	5+8+4	0.567	1.3	2.29	B

Sl no	Sample no	L (cm)	W (cm)	T (cm)	Oxide thickness (mm)	Av oxide thickness(cm)	Nucleus thickness(cm)	Ratio of nucleus to oxide	Type of nucleus
37	F2/74B	4.1	3.1	3	2+5+4	0.367	0.9	2.45	AB
38	F2/96F	6.2	3.8	3.9	11+16+12	1.3	0.7	0.54	MIXED
39	F2/95D	4.8	4.8	3.5	5+4+4	0.433	1.4	3.23	AB
40	F2/95C	3	2.7	1					AB
41	F2/73D	6.6	5.8	3.2	2+4+2	0.267	2.4	8.99	C
42	F2/88	4.1	3.4	3.4					AB
43	F2/79C	4.6	3.3	3.2	11+7+9	0.9	0.7	0.78	C
44	F2/88BC	3.5	3.2	2.7	8+5+7	0.667	1.2	1.80	P
45	F2/80B	6.5	5.2	3.8	3+1+2	0.2	2.4,2.7	0.08	C
46	F3/103D	4.8	3.3	3	3+4+2	0.3	0.9	3	C
47	F2/97F	4.6	3.7	3.5	4+3+2	0.3	1.2	4	C
48	AAS3/B15/55	7.2	6.2	3.1	6+2+2	0.333	1.7	5.10	P
49	F6/3274B	5.9	3.6	3.6	5+8+7	0.667	2	3	C
50	F1/61D	6	4.7	2.3	8+4+6	0.6	0.7	1.17	AB
51	F1/37B	7.7	5.6	5.3					AB
52	F1/60D	5.3	3.3	2.2	1+2+2	0.167			AB
53	F1/18A	5	4.4	3.8					AB
54	F14DRDG	5.8	3.6	2.7					AB
55	GR1/23B	4.7	4.3	3.8	9+35+5	0.5833	0.5	0.86	AB
56	GR1/11A	5.8	4.7	2.8	35+35+35	0.35	0.9	2.58	AB
57	GR1/9C	6.8	3.8	3	2+2+2	0.2	1.8	9	AB
58	GR1/13D	5.1	4	3.2	55+4+3	0.483	1,1.1	0.48	AB
59	SS6/423B	6	4.6	2	1+2+2	0.167	1.4	8.38	MIXED
60	SS6/372J	4	4	3.6	10+12+9	0.733	0.3	0.41	AB
61	SS3/193F	3.5	3	3.+	10+9+13	0.767	0.4	0.52	AB
62	SS6/390D NOD	4.7	3.3	2.3	3+3+3	0.3	1.2	4	AB
63	SS6/390D CRUST	7.4	4.3	2.1	1+2+1	0.133	1.5	11.28	AB
64	SS5/311C	5.4	4	4.3	4+3+3	0.333	1.7	5.10	B
65	SS15/783A	3.5	2.6	2.8	4+3+4	0.367	1.6	4.36	B
66	SS5/301H	4.1	3.2	2.5	3+2+5	0.333	0.8	2.40	B
67	SS9/568ABC	4	3.8	2.8	6+9+3	0.6	0.7	1.17	AB
68	SS5/351B	6.3	3.6	3.4	4+3+3	0.333	2.5	7.51	C
69	SS7/463E	4	3	2	5+3+5	0.433	1.1	2.54	AB
70	SS9/556AB	4.7	3.5	3					AB
71	SS9/618AB	5.9	4.7	3.3	11+8+1	0.967	.9,1.2	0.92	AB
72	SS16/868F	3.3	3	2.3	6+4+8	0.733	1.1	1.50	B
73	SS2/110C	3.5	2.8	1.5					AB
74	SS3/147G	6	4.7	2.1	6+1+2	0.3	1.1	3.67	AB
75	SS13/684	4	3.8	3					ST

Sl no	Sample no	L (cm)	W (cm)	T (cm)	Oxide thickness (mm)	Av oxide thickness(cm)	Nucleus thickness(cm)	Ratio of nucleus to oxide	Type of nucleus
76	SS6/374E	6.8	5.2	4.3	4+8+3	0.5	1.9	3.8	MIXED
77	SS14/710C	5.5	3.5	3.3	4+5+7	0.533	1.6	3.	AB
78	SS13/691A	3.8	3.4	3	3+2+2	0.233		0	AB
79	SS14/717A	6.2	6.2	5.8					MIXED
80	SS4/216B	5.4	2.8	2.8	5+4+8	0.567	1.1	1.94	AB
81	SS9/621C	8.6	9.6	4.3					ST
82	SS15/766A	3.1	3.4	2.5	2+1+3	0.2	0.8	4	AB
83	SS9/559A	5.4	5	3.5	2+2+3	0.233	1.7	7.29	B
84	SS11/664C	9.1	8.3	5.7					MIXED
85	SS15/771A	3.6	3.2	3					AB
86	SS10/655B	4	3	2.5	1+2+1	0.133	0.7	5.26	AB
87	SS16/823C	4.5	3.4	2.3	very thin	very thin			P
88	SS15/776D	6.7	7	0.9	5+9+8	0.733	VERY SMAL		C
89	SS9/569AB	6.3	4	3.7	2+3+2	0.233	2	8.58	B
90	SS3/162D	4.5	3.7	3.6	6+2+5	0.433	0.6	1.38	U
91	SS8/511D	6.1	5.7	3.5	4+8+11	0.767	1.3,.6	0.80	AB
92	SS5/309ABC	9.3	6.2	3.4	4+3+3	0.333	1.2	3.60	C?
93	SS4/280F	7	8.1	4.3	13+3+8	0.8	1.2	1.5	ST
94	SS9/597B	6.2	6.4	5.3					AB
95	SS2/107A	4.5	3.5	2.2	3+4+2	0.3	0.7	2.33	AB
96	GR3/123F	3.5	2.5	1	10+9+9	0.933		0	U
97	GR3/112C	4	3.5	2.7	7+12+9	0.9	0.8	0.89	C
98	GR3/121A	4.2	3	2.9	2+2+3	0.233	2.3	9.87	C
99	GR3/99C	8	6	2.3	3+4+5	0.4	1.1	2.75	C
100	GR3/129B	3.9	3.7	3.1	4+3+5	0.4	1.6	4	B
101	SS3/167C	5.9	5.7	4.3					B
102	SS14/733D	4.2	3.9	2.9	4+4+7	0.5	1	2	AB
103	SS16/790B	4.3	4.1	4.1	4+4+2	0.333	2.5	7.51	B
104	SS16/814C	8.5	8.3	3.7	12+10+2	0.8	2.4	3	ST
105	SS15/743A	4.9	4.7	2.2	3+1+1	0.167	0.8	4.79	AB
106	SS9/619C	8.1	8.4	6	5+3+3	0.367	2.3	6.27	AB
107	SS9/624AB	5	4.4	3.5	2+1+3	0.2	1.2	6	AB
108	SS16/789F	4.3	4	3.3					AB
109	SS3/190ABCDEF	3	3	2.5	3+8+10	0.7	1	1.43	AB
110	SS14/708BCEG	3.7	3.4	3.1					B
111	SS3/183H	3.6	3	1.8	7+2+3	0.4	0.5	1.25	AB
112	SS2/74C	2.2	2	1.8					AB
113	SS6/404D	3.9	3.1	2.4	6+5+3	0.467	1.5	3.21	AB
114	SS4/254G	4.8	3.6	2.2	2+2+1	0.167	1.3	7.78	AB

Sl no	Sample no	L (cm)	W (cm)	T (cm)	Oxide thickness (mm)	Av oxide thickness(cm)	Nucleus thickness(cm)	Ratio of nucleus to oxide	Type of nucleus
115	SS11/663W	6	4.6	4.7	21+8+13	1.4	1.1	0.78	B
116	SS3/182AG	3	2.7	0.6					AB
117	SS8/521B	7.8	4.5	3.8	2+3+4	0.3	3.1	10.33	B
118	SS13/704B	7.4	6.3	2.7	1+1+2	0.133	2.3	17.29	C
119	SS6/372E	4.1	3.4	3.2	7+3+4	0.467	0.6	1.28	C
120	SS4/280F	4.2	4.2	3.6	8+4+11	0.767	2.2	2.87	AB
121	SS13/699	7.3	5.7	3.6	7+12+11	1	1.5	1.5	C
122	SS10/650G	8.9	3.8	5.5	6+2+3	0.367	4.3	11.71	C
123	SS8/506A	5.1	3.7	2.9	2+1+2	0.167	1.2	7.18	B
124	SS2/87B	4.5	3.4	2	3+2+1	0.2	1.1	5.5	AB
125	SS11/669H	5	2.5	1.1	2+1+3	0.2	0.5	2.5	B
126	SS11/664L	5.5	5.6	1.5	very thin	very thin			C
127	SS3/191F	4.8	3.3	2.7	2+2+2	0.2	1.6	8	AB
128	SS3/157C	4.7	3.6	3.4	3+5+4	0.4	1.6	4	AB
129	SS2/92A	5.9	4.1	3.1	1+2+1	0.133	2.7	20.30	AB
130	SS9/557C	4	3.4	3.1	6+6+6	0.6	1.2	2	AB
131	SS16/820G	7.5	4.1	1.5	2+3+4	0.3	0.8	2.67	AB
132	SS9/603A	5.8	6	5.3	9+6+4	0.633	2.2	3.47	B
133	SS14/716AC	4.9	3.8	3	6+12+7	0.833	1.4	1.68	C
134	SS14/721B	3.4	2.6	2.5	5+7+9	0.7	1.1	1.57	AB
135	SS3/134F	5.2	5	2.9					AB
136	SS2/129C	5.7	4.3	3.2	7+14+11	1.067	1.1	1.03	AB
137	S13/682	10.9	3.8	3	2+2+1	0.167	1.8	10.78	AB
138	SS3/184G	5.8	3.4	3.4	18+12+9	1.3	0.2	0.15	AB
139	SS11/670J	4.8	4.4	3.3	9+6+6	0.767	1.2	1.56	C
140	SS9/552A	5.3	4.7	4.9	11+14+4	0.967	3,4	2.76	AB
140	SS5/330ACDE	6.6	4.7	3.1	6+5+15	0.867	1.6	1.84	AB
142	SS10/657	4.8	4.5	4					AB
143	SS11/665A	6.3	5.3	3.8	26+15+1	0.17	0.6	3.53	C
144	SS15/762A	5.8	2.6	2.5	1+2+6	0.3	1.2	4	U
145	SS16/826E	5.4	4.3	4	94+72+84	0.833	2.16	2.59	B
146	SS10/NOD FROM PRE	4.6	4	3.3	3+3+1	0.233	1.6	6.87	AB
147	SS11/665A	9.4	5.6	3.7	4+5+3	0.4	3.1	7.75	S
148	SS4/250F	2.9	2	2	2+1+3	0.2	1.3	6.5	AB
149	SS3/167G	5	4	3.4	5+8+7	0.667	1.3	1.95	C
150	SS15/781D	3.8	2.3	2.1	7+6+4	0.567	0.8	1.41	AB
151	SS15/753B	5	3.6	3	3+4+2	0.3	1	3.33	AB
152	SS10/653C	4.5	3.4	2.6	2+3+2	0.233	1.6	6.87	C
153	SS13/692B	5.2	4	2.9	1+1+1	0.1	0.2	2	U

Sl no	Sample no	L (cm)	W (cm)	T (cm)	Oxide thickness (mm)	Av oxide thickness(cm)	Nucleus thickness(cm)	Ratio of nucleus to oxide	Type of nucleus
154	NR2/101C	3.7	3.7	3.7	2+2+2	0.2	1.1	5.5	AB
155	NR2/69DE	5.5	4.6	4	1+2+1	0.133	1.3,1.5	0.09	AB
156	NR1/22C	7	4.7	4.5	16+6+12	1.2	0.8	0.67	AB
157	NR2/83AB	7.5	6	2.7	10+10+7	0.9	0.55	0.61	C
158	NR3/126B	5.4	3.6	3	3+3+3	0.3	1.1	3.66	AB
159	NR2/71D	3.2	2.4	1.7	3+6+1	0.333	1	3.00	AB
160	NR3/128A	5.6	4.9	3.3	2+1+2	0.167	2.2	13.17	B
161	NR1/47C	5.3	4.3	3.7	4+3+3	0.333	0.6	1.80	B
162	NR2/101AB	5.5	3.8	3.4	3+4+3	0.333	1	3.00	AB
163	NR4/158D	6.7	5.2	3.6	2+2+2	0.2	2.4	12	B
164	NR1/47C CRUST	11.3	7.2	3.9	2+4+1	0.233	2	8.58	AB
165	NR4/158BC	11.9	6.8	3.3	2+1+2	0.167	2.7	16.17	C
166	NR3/128E	4.3	4.1	2.9	6+3+9	0.6	1.2	2	MIXED
167	NR4/158D	4.8	3.7	3.4	1+2+2	0.167	2.9	17.36	AB
168	NR3/126E	4.7	3.8	2.3	4+1+2	0.233	1.5	6.438	AB
169	NR3/126E1	3.4	2.6	2.1	2+5+3	0.333	1.2,1	0.302	AB
170	NR2/90E	4	2.8	1.9	6+5+9	0.667	0.7	1.05	B
171	SS9/592C	14	9	6.5	18+19+13	1.667	3.5	2.1	C

Table 4a.

Oxide	Nucleus	Near nucleus	1	2	3	4	5	6	7	Near boundary
Na <sub>2</sub> O	-	-	2.14	-	6.47	4.91	5.54	3.4	7.24	-
MgO	3.4	2.72	2.53	4.13	7.37	5.66	7.12	5.46	7.48	1.61
Al <sub>2</sub> O <sub>3</sub>	12.48	6.88	6.72	5.09	6.28	4.52	5.26	4.97	4.05	1.19
SiO <sub>2</sub>	53.03	52.25	21.15	9.74	10.58	5.75	3.6	5.31	2.34	-
K <sub>2</sub> O	3.45	0.76	1.08	0.9	1.31	1.16	1.02	1.65	1.33	1.47
CaO	-	1.15	2.99	2.31	1.75	1.79	2.06	1.79	2.34	2.29
MnO	2.62	29.15	43.68	61.36	61.27	69.32	69.5	71.25	68.6	87.04
Fe <sub>2</sub> O <sub>3</sub>	24.15	4.56	15.26	11.79	-	-	-	-	-	-
NiO	-	1.88	1.35	3.26	3.56	5.07	4.13	4.17	4.74	4.05
CuO	-	0.65	0.58	1.42	1.41	1.83	1.3	1.99	1.88	2.36

Table 4b.

Oxide	inner cusp	outer cusp
Na <sub>2</sub> O	4.11	2.2
MgO	1.97	1.43
Al <sub>2</sub> O <sub>3</sub>	6.44	3.89
SiO <sub>2</sub>	31.5	19.12
K <sub>2</sub> O	0.61	0.64
CaO	2.59	2.34
MnO	24.14	33.62
Fe <sub>2</sub> O <sub>3</sub>	27.63	35.51



Table 5.

Oxide	On botryoid	Section of botryoid	Away from botryoid
Na <sub>2</sub> O	-	3.37	5.05
MgO	1.94	1.5	2.85
Al <sub>2</sub> O <sub>3</sub>	4.9	6.28	4.54
SiO <sub>2</sub>	13.79	11.25	14.05
K <sub>2</sub> O	0.72	0.72	0.64
CaO	2.91	2.99	3.18
MnO	38.05	37.83	37.46
Fe <sub>2</sub> O <sub>3</sub>	36.05	33.23	30.87
CoO	-	0.95	-

Table 6.

Oxide	Pumice 1	Pumice 2
Na <sub>2</sub> O	4.2	4.17
Al <sub>2</sub> O <sub>3</sub>	15.69	13.7
SiO <sub>2</sub>	70.98	69.03
K <sub>2</sub> O	3.5	3.33
CaO	1.32	1.03
MnO	-	-
Fe <sub>2</sub> O <sub>3</sub>	4.3	8.74

Table 7.

Oxide	1	2	3
Na <sub>2</sub> O	2.54	2.09	3.72
MgO	3.27	2.51	3.71
Al <sub>2</sub> O <sub>3</sub>	16.83	16.91	17.74
SiO <sub>2</sub>	40.07	42.02	50.05
K <sub>2</sub> O	0.67	0.7	0.64
CaO	10.92	13.89	10.73
MnO	-	1.6	-
Fe <sub>2</sub> O <sub>3</sub>	23.72	19.06	11.96